63-3

AFCRL-63-73

INVESTIGATION OF THERMAL IMAGING TECHNIQUES
FINAL REPORT

Prepared by

Tibor S. Laszlo
Paul J. Sheehan, Jr.

RESEARCH AND ADVANCED DEVELOPMENT DIVISION
AVCO CORPORATION
Wilmington, Massachusetts

RAD-TR-63-7
Contract AF19(604)-7204
Project 4619
Task 46190

15 March 1963

Prepared for

ELECTRONICS RESEARCH DIRECTORATE
AIR FORCE CAMBRIDGE RESEARCH LABORATORIES
OFFICE OF AEROSPACE RESEARCH
UNITED STATES AIR FORCE
Bedford, Massachusetts

AFCRL-63-73

This document consists of 108
90 copies, Series A

INVESTIGATION OF THERMAL IMAGING TECHNIQUES
FINAL REPORT

Prepared by

Tibor S. Laszlo
Paul J. Sheehan, Jr.

RESEARCH AND ADVANCED DEVELOPMENT DIVISION
AVCO CORPORATION
Wilmington, Massachusetts

RAD-TR-63-7
Contract AF19(604)-7204
Project 4619
Task 46190

15 March 1963

Prepared for

ELECTRONICS RESEARCH DIRECTORATE
AIR FORCE CAMBRIDGE RESEARCH LABORATORIES
OFFICE OF AEROSPACE RESEARCH
UNITED STATES AIR FORCE
Bedford, Massachusetts

Requests for additional copies by Agencies of the Department of Defense, their contractors, and other Government agencies should be directed to the:

ARMED SERVICES TECHNICAL INFORMATION AGENCY
ARLINGTON HALL STATION
ARLINGTON 12, VIRGINIA

Department of Defense contractors must be established for ASTIA Services or have their "need-to-know" certified by the cognizant military agency of their project or contract. All other persons and organizations should apply to the:

U. S. DEPARTMENT OF COMMERCE

OFFICE OF TECHNICAL SERVICES

WASHINGTON 25, D. C.

ABSTRACT

Experiments and measurements which can be performed successfully in image furnaces are listed together with the necessary special instrumentation. The restrictions imposed by basic principles of image furnaces upon their operation are discussed, and methods to overcome these restrictions are proposed. Sample holders were designed and built which permit operation in controlled atmospheres with rotation of the sample on, or perpendicular to the optical axis, and which are suitable for the measurement of electrical properties at high temperatures. A fast action, on-off shutter has been designed to be operated by compressed air and vacuum. A new guidance control system has been built having greater sensitivity and precision than the previous model. An experimental setup has been constructed for the direct measurement of solar reflection coefficients. A 36-inch paraboloidal reflector has been fabricated by a new method. A method has been developed which makes it possible to calculate the temperature dependence of a property from measurements of the uneven flux distribution of the image at several peak flux values. Blackbody cavities are discussed, and a new shape blackbody is presented which absorbs a larger portion of the incident radiant energy than previously known shapes. Analytical evaluation for this shape was made and compared with results for previously known shapes. A calorimeter was built using this shape and fluxes in the solar furnaces were measured with it. The resultant correlation of normal-incidence solar radiation and the concentrated flux in the focal area is presented. The use of the solar furnace as a high-intensity radiant-flux standard is proposed. The flux distribution was measured with a fine resolution radiometer using MgO-coated absorbing surface. A method for the determination of the sensitivity of the radiometer using a single flux measurement has been developed. Photomicrographs of high-melting point ceramics, melted in the rotating sample-holder, are presented. Single crystals of thoria grown by vapor condensation are shown. A method for the measurement of the electrical resistivity of refractory oxides was developed. A survey of image-furnace facilities has been made.

CONTENTS

ILLUSTRATIONS

ILLUSTRATIONS (Concl'd)

I. INTRODUCTION

Image furnaces are highly suitable for high-temperature experimentation and measurements.[1] For successful operation, however, it is important to consider the unusual heating conditions which exist at the focal area. In most cases, conventional instruments and techniques cannot be used because of the small size and uneven flux distribution of the image. Another restriction of operating conditions is the fact that heating takes place only at the front surface of the specimen. In order to overcome these difficulties, completely new methods and instruments must be devised in many cases to accomodate the unusual space and radiation conditions in image furnace.

Recognizing this need, the Air Force Cambridge Laboratory awarded contract AF 19(604)-7204 to Avco RAD on 16 February 1960 calling for the investigation of requirements for a precision solar imager and for the development of thermal imaging techniques to be used in high-temperature refractory-materials research.

For administrative reasons a report on this work was issued at the end of the first year.[2] The present report also includes all the material of the previous report.

The following scientists and engineers participated in the reported work: Tibor S. Laszlo, (principal investigator); Murray S. Klamkin, Salvatore Motta, Paul J. Sheehan, Jr., Arthur W. Shores, and Royal N. Schweiger. The contract was monitored by Mr. George P. Ploetz, CRRCPS. The experimental work was performed on the Avco RAD 60-inch solar furnace shown in figure 1.

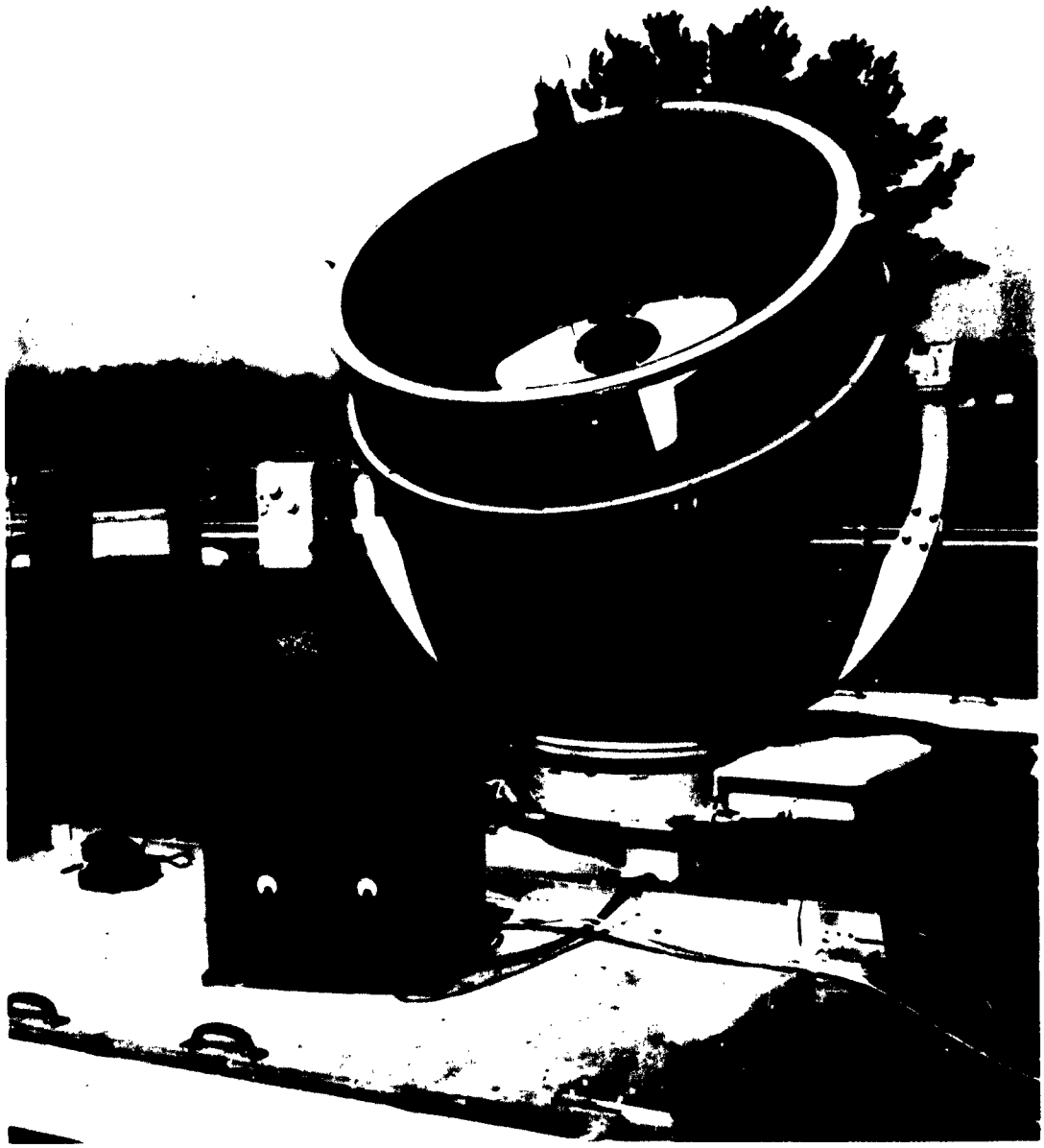

Figure 1 AVCO RAD SOLAR FURNACE
P-59-1192

II. DESIGN AND OPERATING PARAMETERS

In order to select the most important experimental and instrumentation problems for the present investigations, a survey was prepared defining the field of activity for image furnaces. Only such work as would benefit by the special advantages of image furnaces was considered, as were areas where there appeared to be a reasonable probability of overcoming restrictions specific to image furnaces. In the following, the suggested experiments are listed together with the needed accessory equipment. All listings are cumulative.

A. MEASUREMENT OF PHYSICAL PROPERTIES

1. Temperature

Required: Sample positioning in the three spatial coordinates, observation hole at the optical axis, flux control, separation of radiation emitted by and reflected from the sample, and manual or recording optical pyrometer or radiation pyrometer designed for the aperture existing in the furnace.

2. Emissivity

Required: Watercooled, calibrated radiometer on a semicircular mount, permitting measurement at any angle up to 90 degrees off the optical axis, monochromator for spectral emission measurement, and artificial blackbody for reference.

3. Melting Point

Required: Controlled atmosphere sample holder with rotating sample mount, provision for removal of condensations from window, and telescope for sample observation.

4. Thermal Expansion Coefficient

Required: Controlled atmosphere sample holder to rotate the sample normal to the optical axis, reflector behind the sample, and specially designed optical cathetometer.

5. Electrical Resistivity

Required: Liquid-cooled, rotating copper contacts with keyed faces, sliding contacts, and standard measuring instrumentation.

6. Dielectric Constant

Required: Resonant cavity dielectrometer modified for image furnace use.

7. Thermionic Emission

Required: Vacuum sample holder for closely spaced systems, specially designed contacts with standard potential, and current measuring instruments.

8. Evaporation Rate

Required: Controlled atmosphere sample holder with provision for removal of material, and fast action shutter.

9. Magnetic Susceptibility

Required: Thermally shielded electromagnetic equipment, contacts, and standard instruments.

10. Radiation Standard

Required: Water-cooled radiation calorimeter with differential thermopiles, thermostat, pumps, and standard instruments.

11. Specific Heat

Required: Copper-block calorimeter fitting into sample holder, special sample suspension, and dropping mechanism.

B. OBSERVATION AND MEASUREMENT OF CHEMICAL PROPERTIES

Required: Mechanism to feed solids, liquids, and gases into a controlled atmosphere reaction chamber, and to remove vaporized products. An inert solid surface to absorb radiant energy for gas-gas reactions. The design and performance of these mechanisms will vary according to the reaction.

C. SPECIAL TECHNIQUES

1. Growing of Single Crystals

Required: Powder feed and seed crystal mount, automatic temperature control monitored by a recording optical pyrometer or a specially designed radiation pyrometer.

2. Zone Refining

Required: Sample mount supporting both ends of the sample rod and rotating it; and mechanism to oscillate the sample mount with adjustable length.

3. High Temperature Fabrication

Required: Mounts for welding thermocouple beads in inert atmosphere, shaping of ceramics, welding ceramics to ceramics or to metals, cutting and casting of refractory materials; electronic position indicator, secondary mirrors of special design, and flux redistributors may also be required.

III. RESTRICTIONS ON THE USE OF IMAGE FURNACES

Image furnaces place certain limitations on experimentation. For successful operation, therefore, it is important to develop special equipment as well as special methods which take these limitations into consideration. In some cases, it is possible to adapt conventional experimental techniques to the restrictions of the image furnace; in others, a completely new approach to the problem must be found.

Three specificities require consideration when one is planning experiments in an image furnace. The first is the small size of the hot zone. In carbon-arc image furnaces the image size can be increased by increasing the anode diameter. The required increase in power requirement, however, and the decrease in focusing precision are limiting factors. In solar furnaces, a large image may be obtained by increasing the size of the reflector. However, the technical problems involved in the building and operation of a large solar furnace are considerable. In addition, it is not possible to manufacture a large paraboloidal reflector, especially one composed of several plane or spherical mirrors, with the same high precision as can be done with a smaller one. It appears that a better solution to this problem is to change experimental techniques so as to make use of a small image. The precision of the measurements is not necessarily affected by the reduction of the size of the heated portion of a sample. If the analogy of the development of microanalysis can be applied here, the decrease in sample size may even increase the accuracy of certain tests.

The second limitation, namely, that heating takes place only on one side of the sample, is more restrictive. Heating in a cavity has been suggested[3] to overcome this difficulty. The refractoriness of the cavity material, however, sets a rather low temperature limit on such a technique. In addition, owing to the presence of the sample in the cavity, it is unlikely that a uniform wall temperature can be reached. With this technique, there is also the danger that the proximity of the hot cavity wall may contaminate the sample. A more promising technique is the rotation of the sample around an axis perpendicular to the optical axis of the image furnace to achieve even heating around the entire circumference.

The third restrictive property, the nonuniform flux across the image area, requires the most serious consideration. Two methods appear to be possible to overcome this difficulty. One experimental approach would apply additional optical elements in an image furnace to decrease or perhaps totally eliminate flux differences. The other approach, as evolved during the present work, uses an experimental technique which, together with a newly developed analytical procedure, permits the calculation of the temperature dependence of a property measured in the nonuniform flux area.

IV. THE SAMPLE HOLDERS

In order to overcome the one-sided heating of a sample, two special sample holders have been designed and built. The first holder is shown schematically in figure 2. The cylindrical transite enclosure is topped by a transparent hemisphere. Generally, a pyrex hemisphere cut from a one-liter, round-bottom flask is used. When the highest obtainable fluxes are required, a clear fused silica or a vycor hemisphere is recommended. An oscillating wiper blade scrapes deposits off the inside of the hemisphere. The wiper blade is made of steel tailored to the shape of the hemisphere and covered with a woven silica-fiber sleeving. The sample can be rotated at variable rpm around the optical axis of the furnace in order to obtain symmetrical heating. Gas inlet and outlet connections are located at the base plate. The method of mounting the hemisphere is illustrated in figure 3. A transite ring surrounds the hemisphere and presses it to the transite cylinder; the ring itself is tied down by bolts to the base plate. The nuts for the bolts are springloaded in order to avoid failure due to differential thermal expansion. A photograph of the completed sample holder is depicted in figure 4.

The second sample holder, which has been built, permits the rotation of a sample perpendicular to the optical axis of the furnace and provides electrical contacts at the two ends of the sample, as shown in figure 5.

Two hollow stainless steel shafts are used as sample support. The cooling liquid is carried through a small tube inside the shafts to the tips and returns in the space between the tube and the shaft. Gold-plated copper contacts are fitted tightly over the tip of the shafts. The faces of the copper contacts are made to fit the sample diameter, and are provided with a key to firmly engage a slot in the end of the sample. One of the shafts is rotated by a servo motor through a gear mechanism while the other rotates freely. The driven shaft can be adjusted laterally to accommodate samples of various length. The other shaft is springloaded in the lateral direction in order to make good mechanical contact with the sample. Through this contact the shaft follows the rotation of the driven shaft. In addition, the springloading facilitates sample insertion and removal. Copper tubes for the cooling liquid connections are mounted on the bearing housings and "0" rings are used to make a liquid-tight rotating seal.

The two rotating shafts are isolated electrically by the use of teflon gaskets underneath the bearing housings which are fastened to the baseplate with nylon-coated screws. Electrical contacts to the rotating shafts are made by the use of nickelplated copper discs silver-soldered onto the shaft and immersed in a container filled with mercury. The mercury container is mounted in such fashion that it can rotate freely around a horizontal axis. By this arrangement, the container will always be in a horizontal position, regardless of the actual pointing angle of the solar furnace. A cover placed over the container, with a

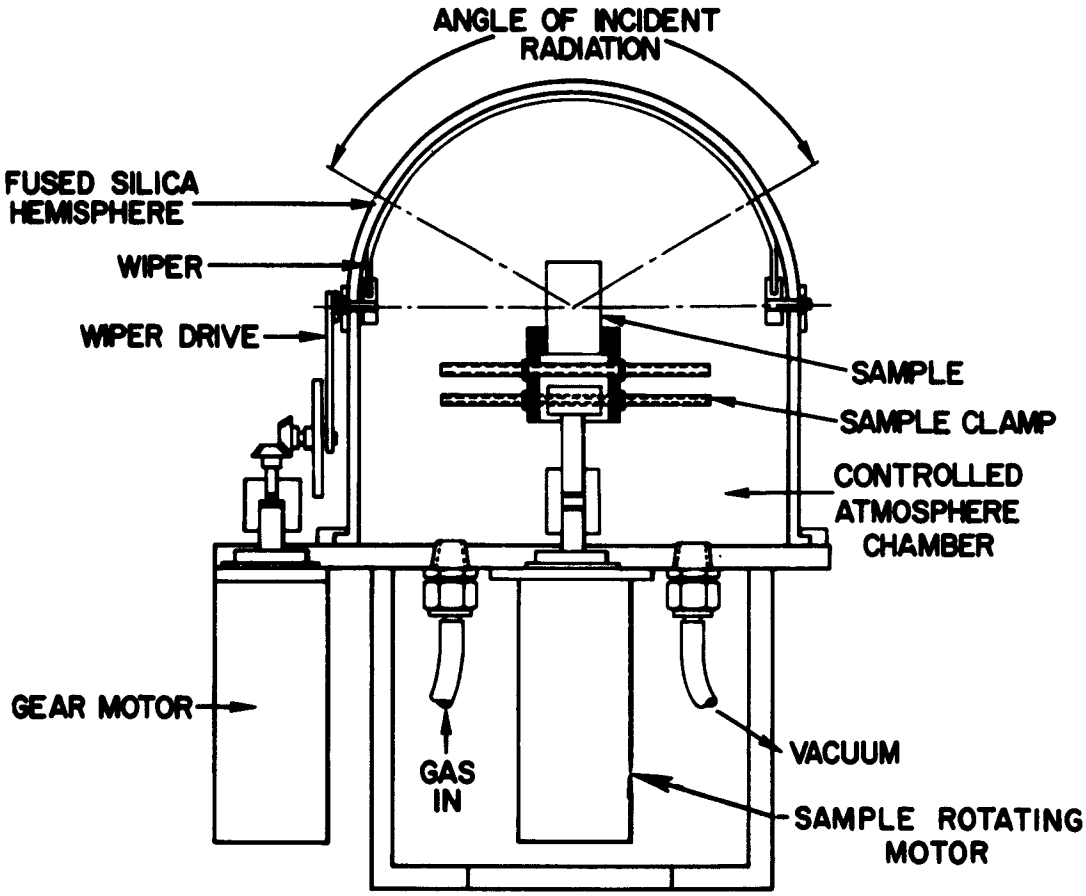

Figure 2 CONTROLLED ATMOSPHERE SAMPLE HOLDER
60-2613A

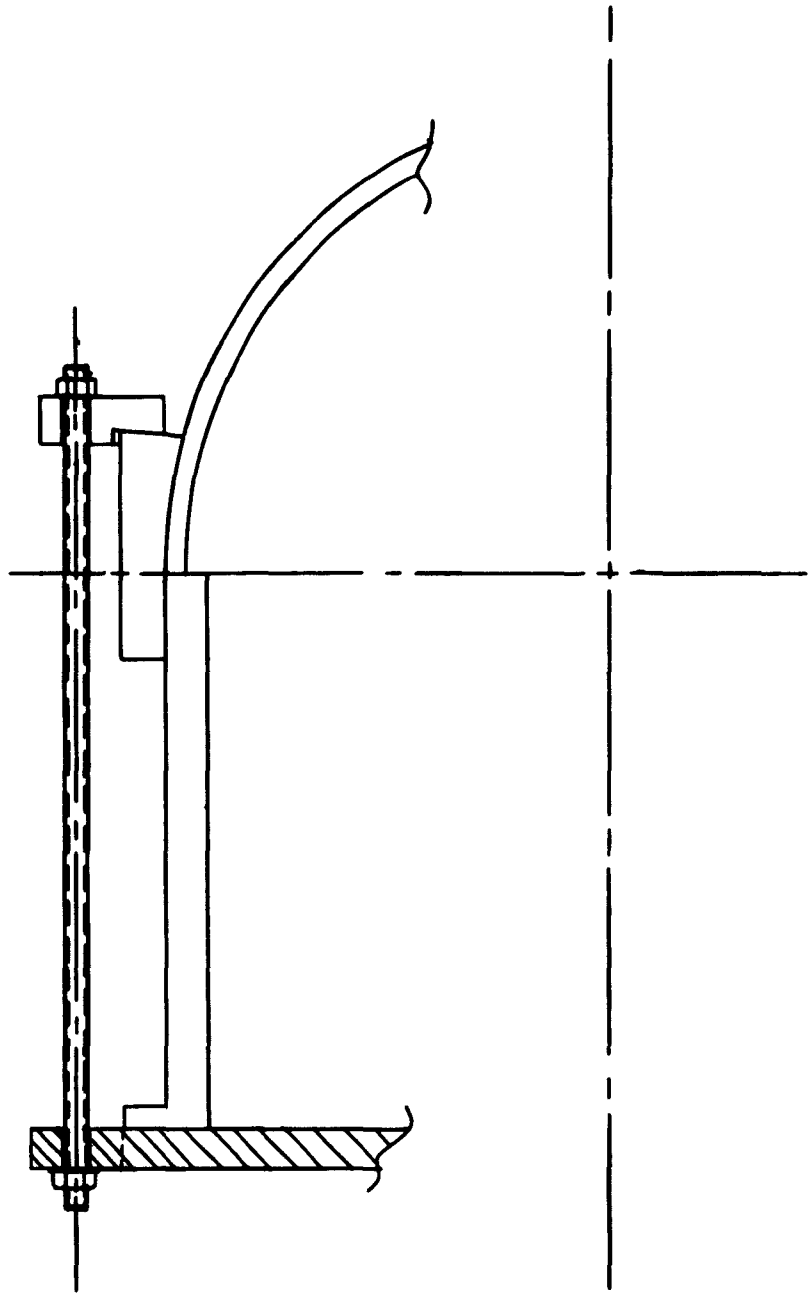

Figure 3 TRANSPARENT HEMISPHERE MOUNT
61-2119

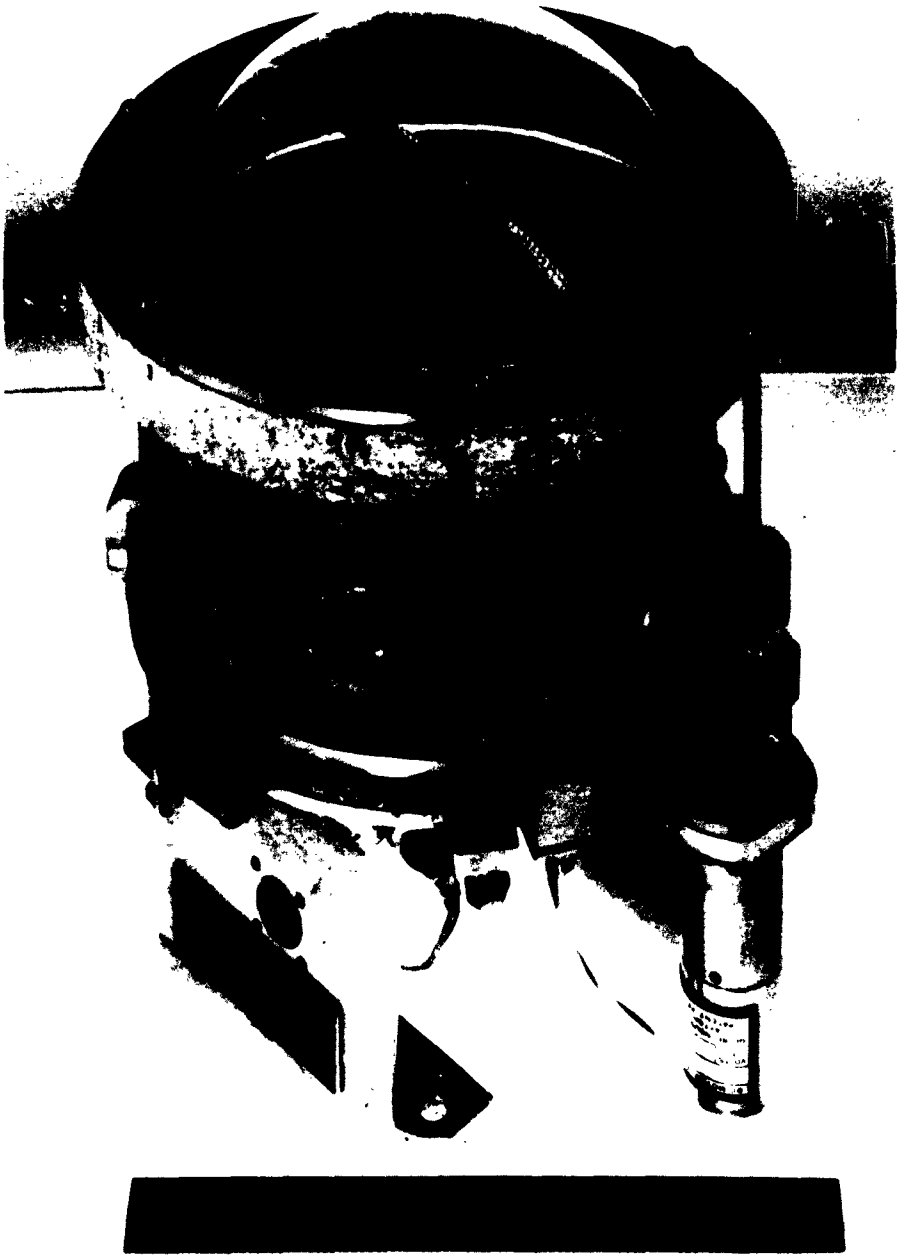

Figure 4 CONTROLLED ATMOSPHERE SAMPLE HOLDER
P-6114

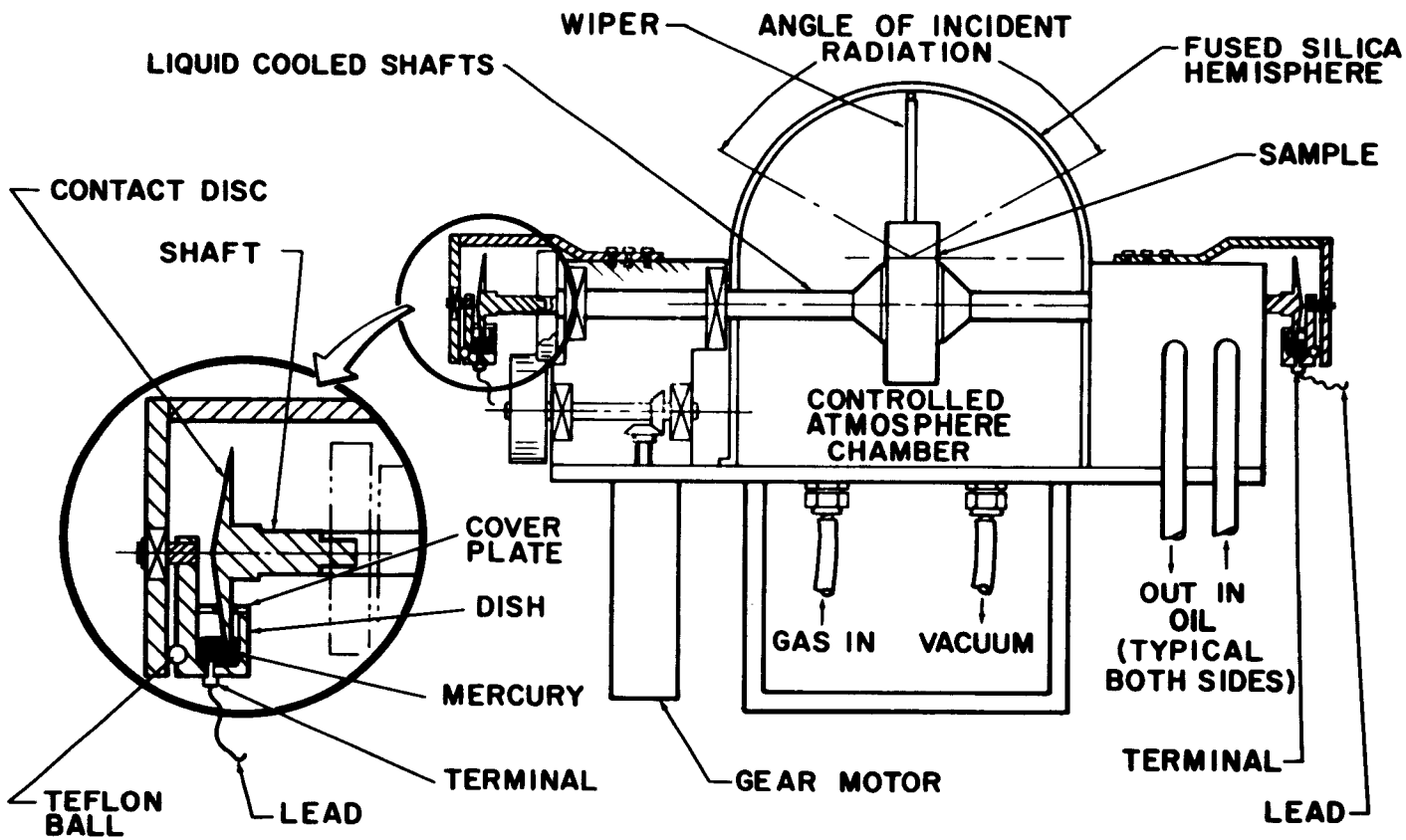

Figure 5 SAMPLE HOLDER FOR ELECTRICAL MEASUREMENTS
62-1395

narrow slit for the rotating disc, keeps contamination of the mercury to a minimum. Any fine dust which finds its way into the container will float at the surface of the mercury without interfering with a good electrical contact. A fine, flexible wire connects each freely moving container to binding posts mounted on the sample-holder base. These posts in turn are connected to the measuring instrumentation installed outside the furnace.

The controlled atmosphere chamber, transparent hemisphere, and wiper mechanism are similar to those used on the first sample holder. Figure 6 is a photograph of the completed apparatus.

The sample holder was tested for electrical conductivity. It was found that the resistance between the terminal and the copper contacts is 2-5 ohms. The resistance between the two opposite copper contacts is $> 10^4$ megohms when the rotating shafts are cooled with transformer oil. These values make the sample holder suitable for the measurement of electrical resistivity in the 1 kohm-100 megohm range. The rotation of the sample perpendicular to the optical axis of the furnace makes it possible to obtain temperature uniformity around the circumference.

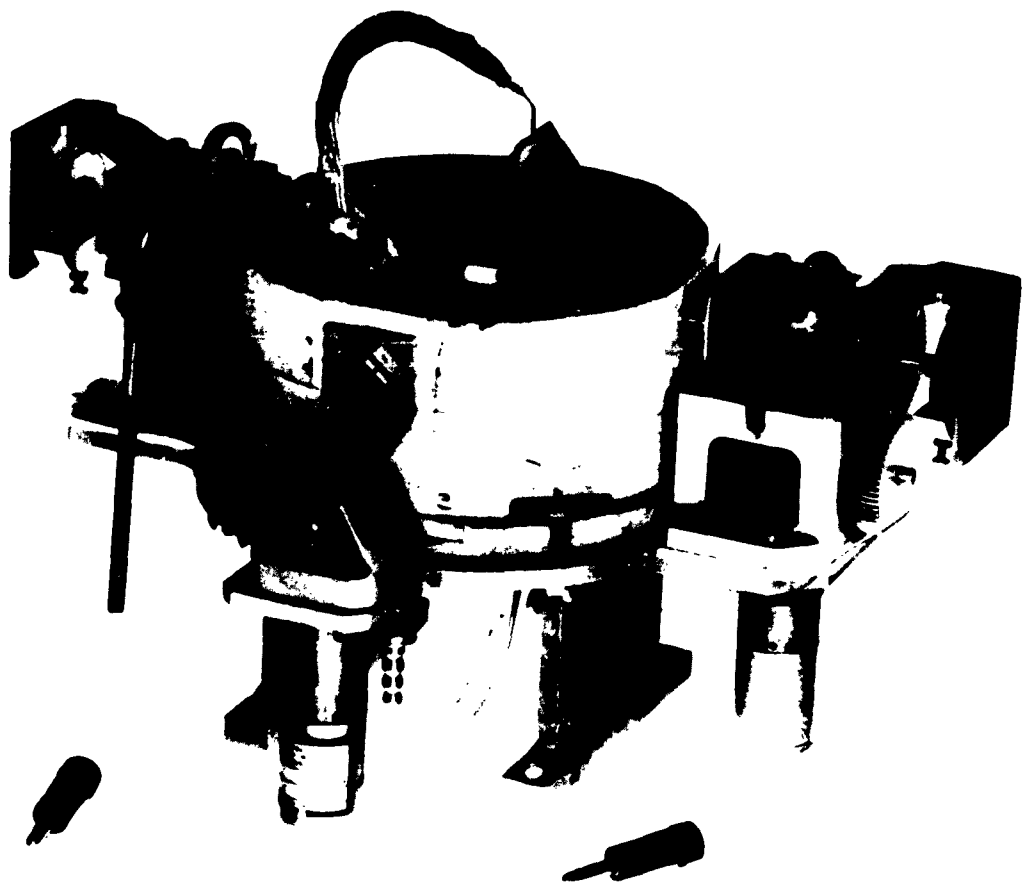

Figure 6 SAMPLE HOLDER FOR ELECTRICAL RESISTIVITY MEASUREMENTS
P-9169

V. THE SHUTTER

In many image furnaces the intensity of the flux impinging on a specimen is controlled by a cylinder moving along the optical axis. For certain experiments, however, an instantaneous on-off flux control is necessary. Venetian-blind-type shutters are now in use on some furnaces[4] which combine the effect of flux attenuation and on-off control. A disadvantage of this mechanism is that, even in the fully open position, it blocks the passage of radiation due to the thickness of the slats and the support members which are needed.

A fast-action, on-off shutter has been designed, which does not cast any shadow on the reflector when in a retracted position. Figure 7 illustrates the mechanism of the shutter. The flux interceptor has a ribbed umbrella-like structure which is supported by a telescoping tube. In its retracted position the entire structure is behind the mirror, and when not needed it can be swung away from the observation hole. It is extended by the application of compressed air and retracted by vacuum. In the center of the telescope structure, there is another telescoping tube, which permits observation of the sample during the entire operation.

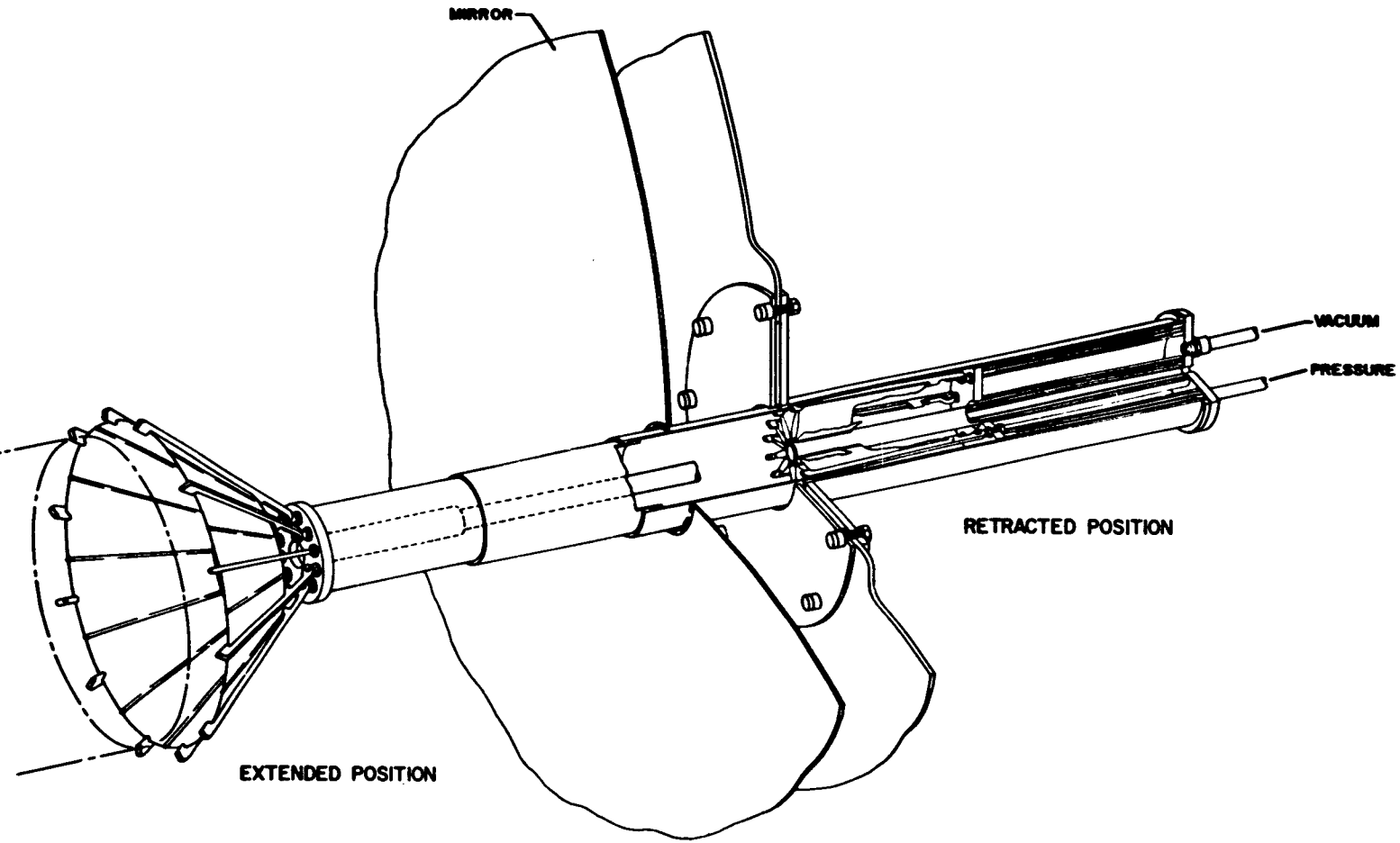

Figure 7 SOLAR FURNACE SHUTTER
60-2615

VI. NEW GUIDANCE SYSTEM FOR SOLAR FURNACES

A new guidance system has been developed for solar furnaces. It has the advantage of being lightweight, inexpensive, highly sensitive, and simple to construct, since off-the-shelf electronic assemblies of proven reliability are used. The system consists of three parts: (1) the sensing unit, (2) the control unit, and (3) the drive motor as shown in figure 8. The sensing unit consists of four 1P41 phototubes mounted at the end of a 22-inch collimating tube having a 1-inch diameter orifice. As the furnace has an altitude-azimuth mounting, two phototubes are aligned parallel to the horizontal axis of rotation of the mirror, and two are mounted parallel to the vertical axis. A filter is mounted in front of the aperture to reduce the intensity of the light falling on the phototubes. An opaque diffusor is directly in front of the phototubes to eliminate the effect of variations in cathode surface sensitivity. The entire sensing assembly is mounted on the furnace housing with the axis of the collimating tube parallel to the optical axis of the paraboloidal mirror. When the mirror is focused on the sun, an image of the aperture falls on the center of the opaque diffusor and provides equal illumination to all four tubes. Any deviation from perfect alignment causes the spot to move off center, and as a consequence unequal amounts of light to fall on the two opposite tubes, which are part of the same circuit. This generates an error signal which is fed to the control unit.

The control unit is composed of two identical modules, one to monitor and control the altitude sensor and drive motor, and the other to monitor and control the azimuth sensor and drive motor. Each module is a Minneapolis Honeywell Brown continuous balance unit number 353170-3, with minor modifications to the input circuitry as shown in figure 8. The modification is identical for both modules. The error signal from the paired phototubes changes the intensity and, if necessary, the polarity of the current output of the balance units. The modulated current is fed into two reversible Minneapolis Honeywell-type 364949-1 motors which drive the furnace rotating gears.

In use, the new guidance system proved to be highly satisfactory. It operates without any discernible backlash or deviation from the true position as observed on an optical indicator. Even when running for several hours, no manual adjustment of the solar furnace was found to be necessary.

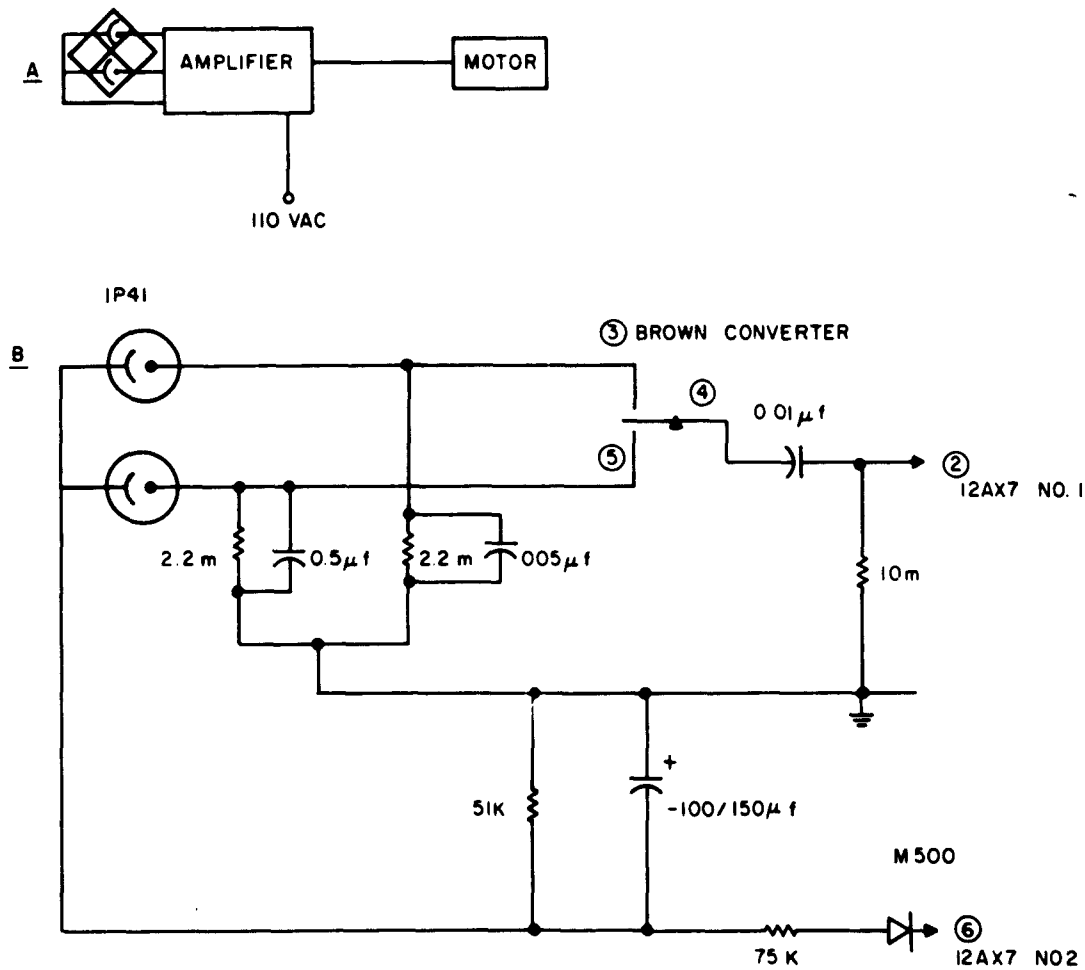

Figure 8 CIRCUITRY MODIFICATION ON MINNEAPOLIS HONEYWELL BROWN AMPLIFIER 353170-3
63-2164

VII. SOLAR REFLECTION COEFFICIENT MEASURING APPARATUS

In the consideration of reflection, absorption, and concentration of solar energy, the knowledge of the solar reflection coefficient is of utmost importance. This optical constant, however, is known only for few materials.[5] Further, the published data have two shortcomings. First, the values have not been measured directly, but rather calculated from spectral data using the weighted ordinate method in the integration for the solar spectrum. Second, the definition of the surface, a very important parameter, is either completely missing or scantily given at best.

An apparatus was therefore designed and built suitable for the direct measurement of solar reflection coefficients using solar radiation as light source. A diagram of the apparatus is shown in figure 9. The measuring instrument is a Hilger radiometer equipped with a collimating tube. In position "A" the radiometer is locked with a springloaded pin in such fashion that its optical axis points at the sun. Thus, the normal incidence solar radiation is recorded. Following this, the radiometer is turned around a pivot into position "B" looking at the sample at 5 degrees off the optical axis. The sample in turn is mounted 5 degrees off the optical axis in the opposite direction. Accordingly, the radiometer in position "B" measures the solar radiation as reflected by the sample. The ratio of the reflected radiation to the normal incidence solar radiation is the solar reflection coefficient. In use, the radiometer output is fed into a recording potentiometer. Since the radiometer can be turned around in a few seconds, one reflectivity measurement can be completed within two minutes, during which time the normal incidence solar radiation is constant under favorable weather conditions.

The alignment of the radiometer, locking pins, sample holder, and pinhole was made on an optical bench to insure accuracy. The entire apparatus was then mounted on the solar furnace in such manner that the optical axis of the instrument is parallel with the optical axis of the solar furnace. As the solar furnace automatically follows the apparent motion of the sun, solar radiation impinges on the sample at exactly 5 degrees. Figure 10 illustrates the apparatus mounted on the solar furnace.

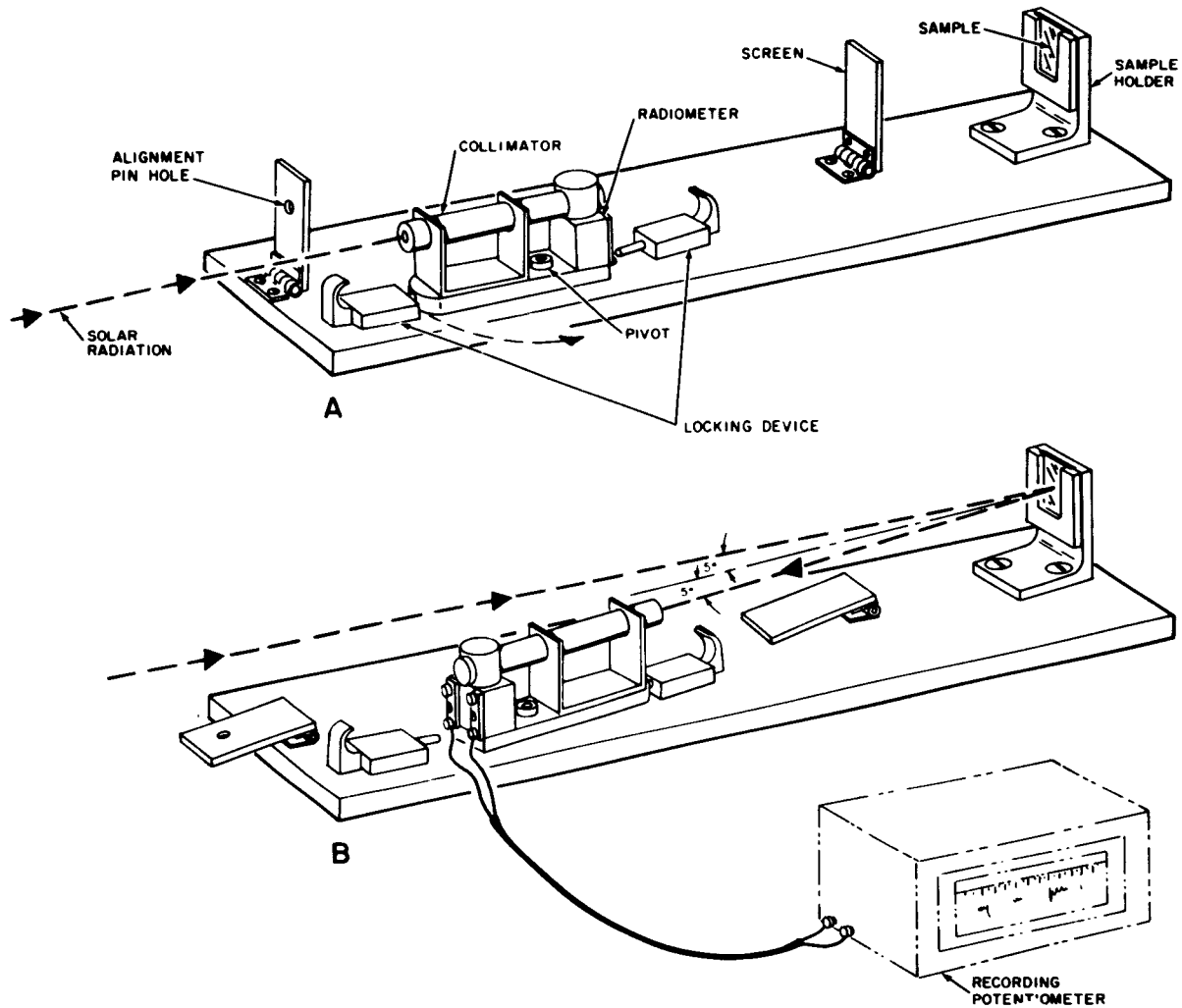

Figure 9 SOLAR REFLECTION COEFFICIENT APPARATUS
(SCHEMATIC DIAGRAM)
61-2569

Figure 10 SOLAR REFLECTION COEFFICIENT APPARATUS MOUNTED ON SOLAR FURNACE
P-6720

VIII. A NEW METHOD FOR THE MANUFACTURE OF PRECISION REFLECTORS

Mirrors in most image furnaces currently in use have been constructed for some other purpose. With few exceptions, either large paraboloidal mirrors from surplus searchlights or ellipsoidal mirrors from motion picture projectors are used. These reflectors are generally of good quality but their greatest advantage is their low cost. The fabrication of reflectors by conventional techniques specifically for use in image furnaces is prohibitively expensive because they are not built in large numbers. Furthermore, the cost increases greatly with a small increase in size. Finally, irrespective of the cost, the required optical precision poses great technical difficulties for large reflector fabrication. Thus, methods for the fabrication of inexpensive precise one-piece paraboloidal reflectors were sought. Several attempts were made earlier to solve the technical difficulties of fabrication at a moderate cost.[6] In these attempts, however, use was made of the availability of a high-precision master. If one were not available the fabrication of the master would involve even more difficulties and greater expense than that of the reflector. These processes, therefore, are justified only if a large number of identical reflectors are required.

It has been found that two recently developed processes, when combined, can be used for the fabrication of inexpensive, precise paraboloidal reflectors with any aperture up to 30 feet. The first process[7] uses the principle that a liquid in a revolving horizontal pan takes the shape of a paraboloid. If a liquid resin, mixed with a hardening agent is thus rotated, a precise paraboloid will be obtained after hardening. A modification of this method was applied in the following process which proved to be suitable for the fabrication of large, precise, and inexpensive paraboloidal mirrors.

A 36-inch diameter aluminum dish, which had approximately the shape of the wanted reflector, was formed by spinning. The centerhole in the metal dish was closed by a wooden plug flush with the inside surface of the metal, and the dish was mounted on a turntable which could be rotated at a precisely controlled angular velocity. A bubblefree mixture of a clear epoxy resin and hardener was poured into the rotating dish enclosed in a dustfree atmosphere. The rotating liquid mixture formed the surface of a paraboloid, its diameter being defined by a rim on the aluminum dish. The paraboloid had a focal length given by

$$f = \frac{1474}{(\mathrm{rpm})^2}$$

The rotation was continued until the resin hardened (approximately 24 hours). During the latter part of the hardening period radiant heat was applied to accelerate the reaction.

The resulting paraboloidal dish had a very smooth, even surface with only a few imperfections visible near the rim. The testing of the dish for geometrical perfection was performed by an optical method illustrated in figure 11. A target pattern consisting of a polar coordinate type graph paper was mounted at the focal point of the paraboloid on three crossways in such a fashion that it could be positioned exactly on the three spatial axes. The target was illuminated with a slide projector placed behind the centerhole of the dish. A wide-angle-lens camera (focal length 19 inches) was located approximately 100 feet from the dish. The camera, the target, slide projector, and paraboloid all were aligned on the same optical axis. Photographs were then taken of the target as reflected by the paraboloidal epoxy surface. The target diameter was much larger than that of the focal area. Therefore, since the focus was well defined, it was necessary to take several photographs with the target in different positions in relation to the focus. Figures 12 and 13 showed the reflection of the target in the epoxy dish photographed at different target-focus relative positions. Some optical distortion was visible on the upper right quadrant of the dish. This distortion indicated such minor local surface inperfections which could not be detected by mechanical means. This quadrant was not used during the successive preparation of the reflecting lining.

The conventional method used to make a reflecting epoxy resin surface consists of the vapor deposition of a metal on it. This process requires a vacuum chamber large enough to accommodate the entire dish, a condition which might be restrictive in the case of large dishes. In addition, it is very difficult to obtain a metal coating which adheres well to the resin and provides a mirror-like finish. Another process was used which is not limited by the size of available vacuum chambers, and in which a highly reflective metal lining is bonded to the resin with an epoxy adhesive. It was necessary then to select that liner material which possesses a suitably high coefficient of solar reflection, durability of finish, and good forming characteristics.

The selection of materials was reduced to two: Alzak finished aluminum and a specially treated, silver-plated copper.* Several tests were performed in order to determine the resistance of the materials to atmospheric corrosion and erosion, and for an estimation of their expected durability as reflector surfaces.

Samples of both materials were subjected to a salt-spray test, the test facility conforming to the requirements of MIL-E-5272. In this test, the sample was placed in a chamber where a finely atomized 18-22 percent sodium chloride solution was circulated freely at 38° C for six hours. Both the silver and the aluminum samples passed this test with only a slight decrease in solar reflectivity as measured with the apparatus described in section VII. A second group of samples was subjected to a sand and dust test conforming to the specifications of MIL-E-5272. The test chamber was maintained at a relative humidity of less than 30 percent, and the sand and dust were circulated with an airstream of 1800-2800 ft/min for one hour at 25° C, and then for one hour at 36° C. The sand and dust concentration was 0.1 and 0.5 g/ft^3, respectively. In this test the silver failed completely while the aluminum showed only a moderate decrease in solar reflectivity.

*Made by Foremost Manufacturing Co., Maplewood, N.J.

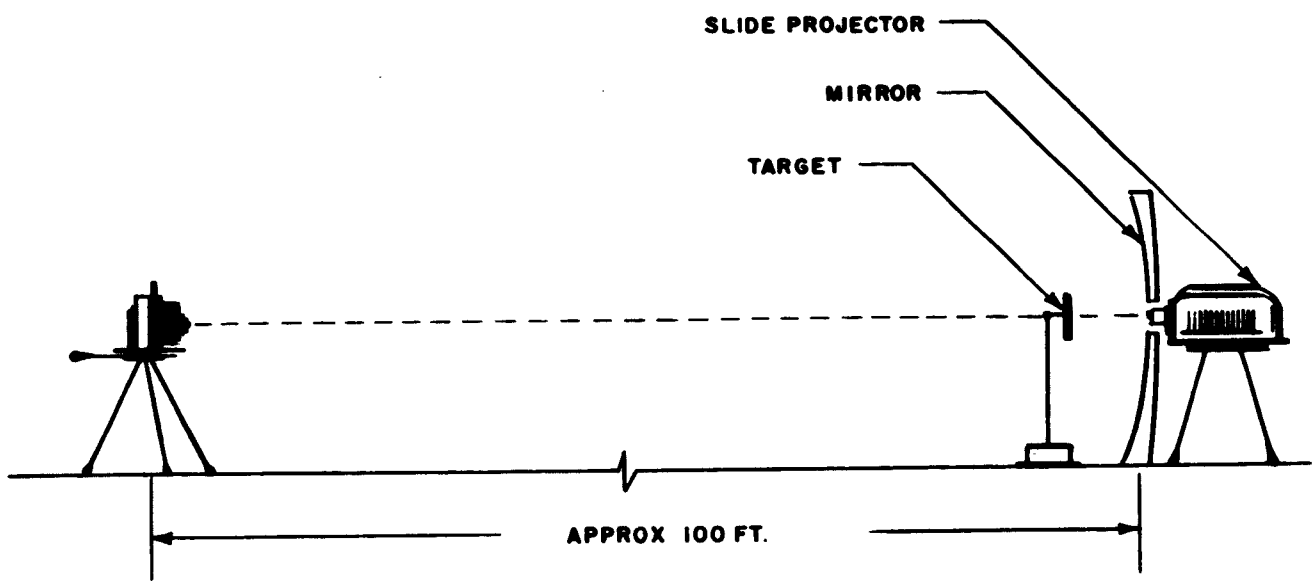

Figure 11 TESTING OF PARABOLOIDAL MIRRORS

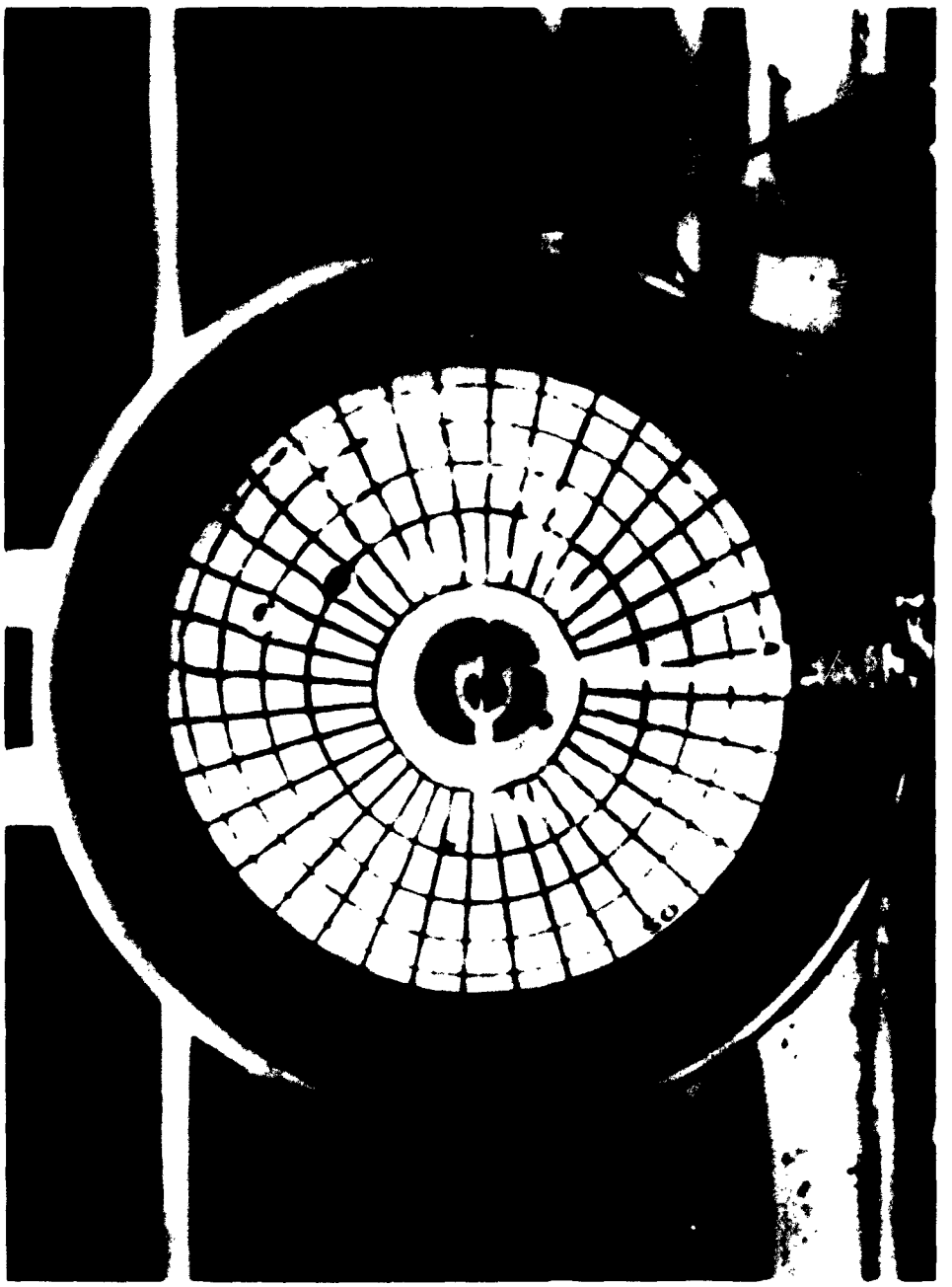

Figure 12 REFLECTED TEST PATTERN

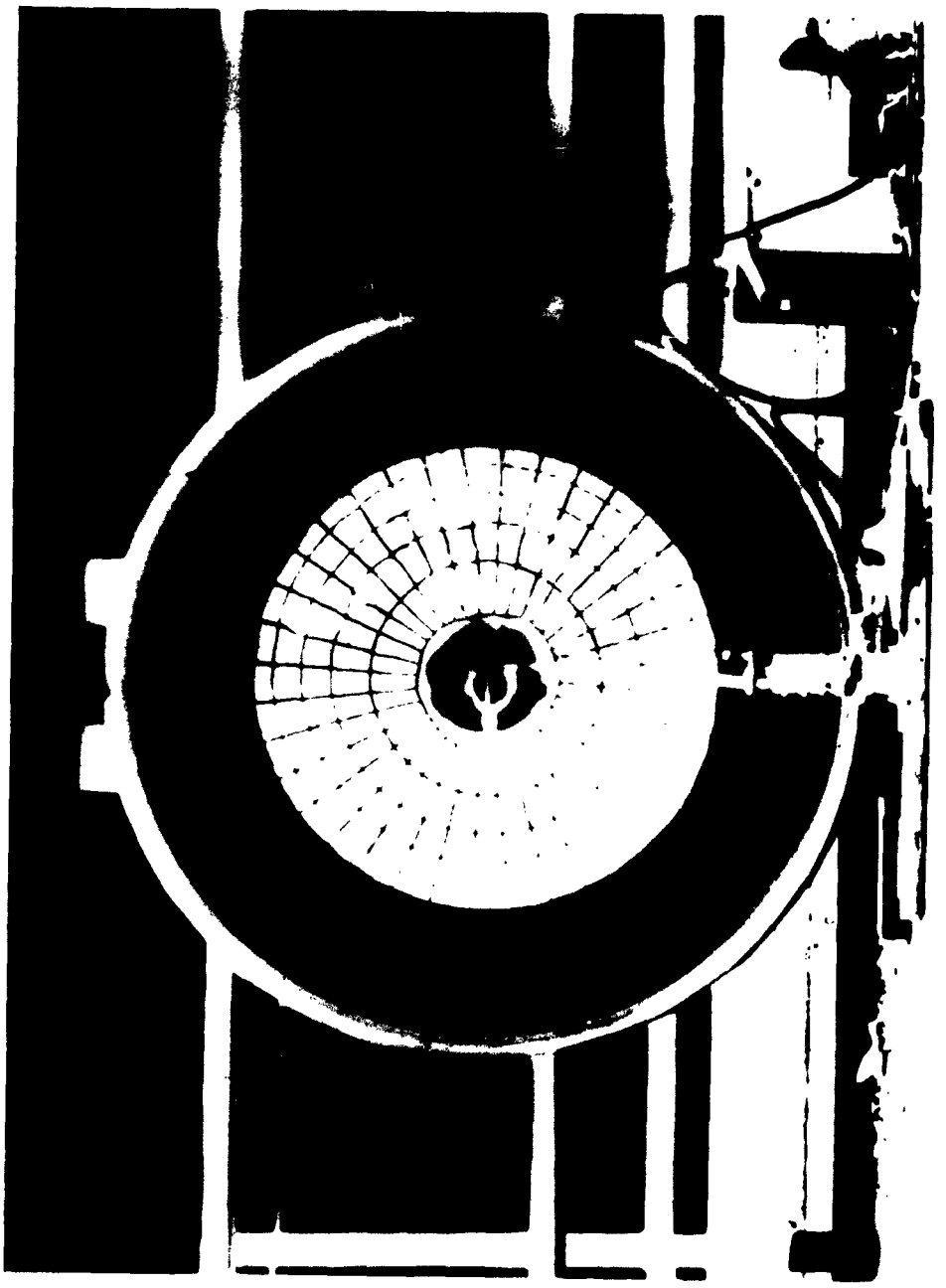

Figure 13 REFLECTED TEST PATTERN

In further test on the Alzak treated aluminum, samples have been exposed to the laboratory and outside atmosphere, respectively, for 64 days. No deterioration of the mirror finish was observed. Another aluminum sample was washed with a detergent and water 63 times without visible deterioration. The same sample, together with a commercial-grade aluminum alloy and a high purity aluminum metal was placed in direct contact with crystals of corrosive sublimate ($HgCl_2$). Within a few minutes, the two latter samples showed corrosion marks and, after 24 hours, deep corrosion pits. The Alzak finished sample did not show any sign of corrosion, even after 24 hours of contact.

Accordingly, the Alzak finished aluminum was selected for the fabrication made. First, a fiber-reinforced plastic casting was made of the most perfect section of the dish. Specially polished 0.035-inch aluminum sheets, prepared for this work at the Alcoa Research Laboratories, were stretch-formed over the casting to obtain petals of the reflector. During the first attempt of stretch forming, the material became so hard it cracked before the desired degree of deformation was reached. It was found that annealing at 445° F relieved the workhardening without adversely affecting the mirror finish. After annealing, eight petals were formed from these sheets and were handpolished in order to remove stretch marks. Following this operation, the sections were Alzak-processed in a colorless electrolyte for the formation of a corrosion-erosion resistant surface. The sections then were trimmed to fit exactly the original epoxy dish and bonded to it with an epoxy adhesive. During the hardening process the petals were pressed into the original dish with a plastic male mold.

The completed paraboloidal reflector was mounted coaxially in the 60-inch solar furnace for testing; figure 15is a photograph of the installation. A fast response radiometer was mounted in the focal area, and the maximum flux in the solar image was located by displacing the radiometer along the three spatial axes until a maximum signal was obtained. Following this, the radiometer was displaced along one of the axes until its output became zero, keeping its position unchanged in reference to the other two axes. Then the radiometer was moved at a constant speed across the image along the same axis, and its output was recorded. The same procedure was followed for the other two axes. The resulting output signals are presented in figure 14. The left-right crossing was made at a higher normal solar incidence than the up-down and in-out crossings, resulting in a greater relative flux intensity. Some irregularity near the mirror periphery is indicated at the edge of the image, but the center portions show a very regular Gaussian distribution. These results are borne out by visual observations. The lines marking the edges of the individual petals are hardly perceptible in figure 15, and the continuity of the image is preserved when it progresses from one petal to an adjoining one. A slight distortion of the curved imageline is visible at the peripheries.

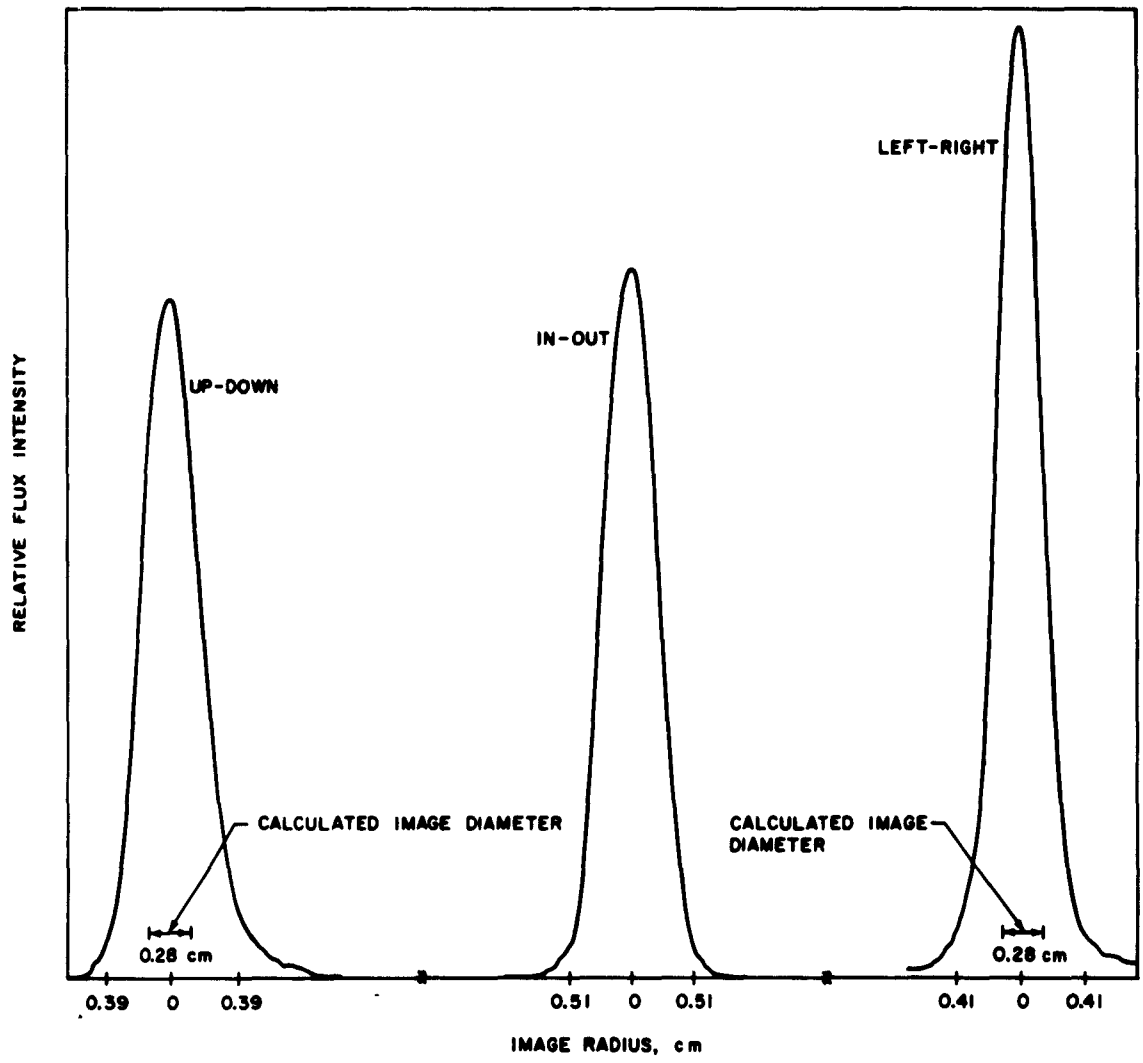

Figure 14 FLUX DISTRIBUTION IN 36 INCH PARABOLOID

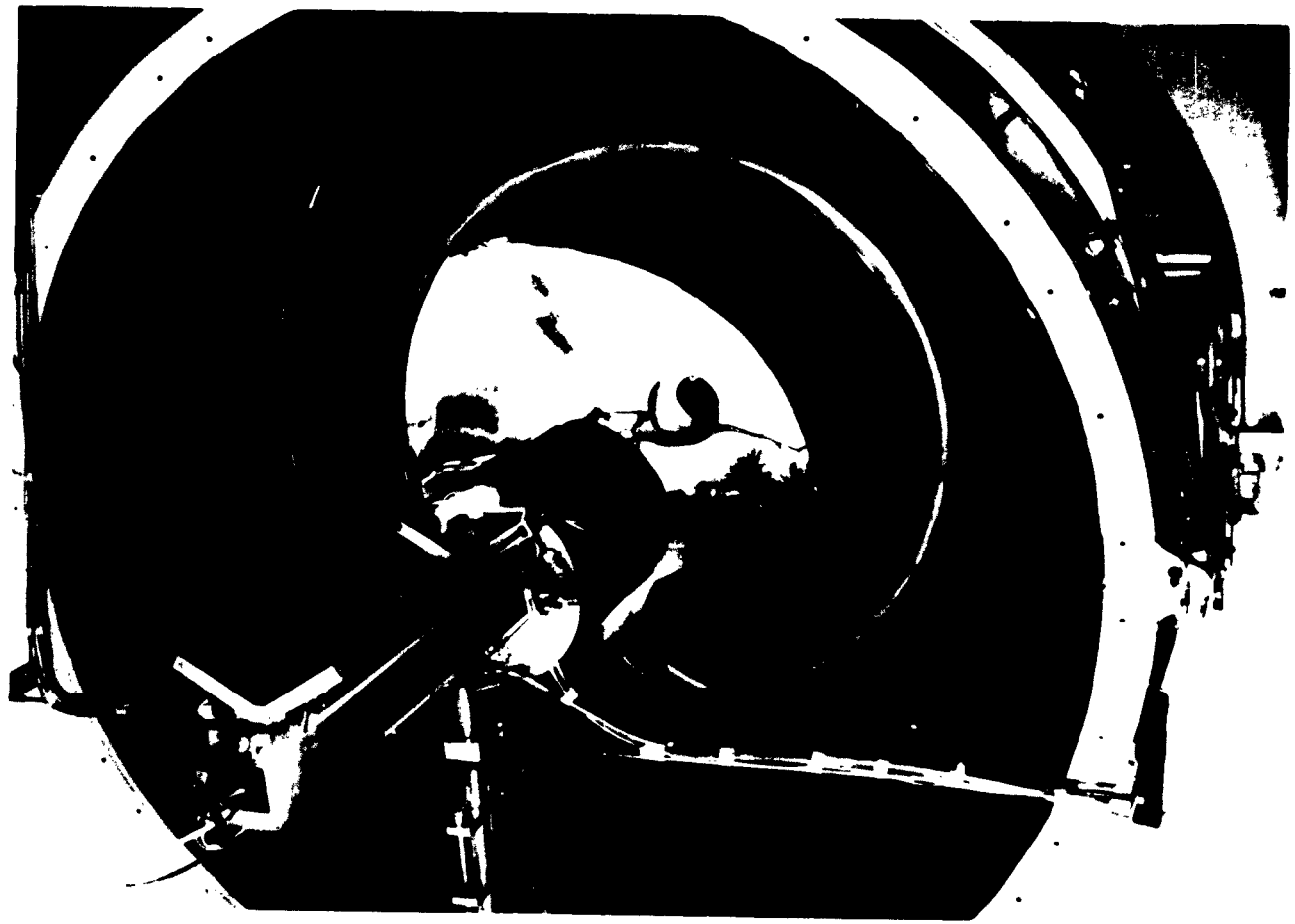

Figure 15 THIRTY-SIX INCH REFLECTOR MOUNTED IN 60-INCH SOLAR FURNACE
P-7984A

This reflector is the first one made according to this new process. It is expected that the experience gained during its fabrication will make it possible to produce reflectors to even better quality. Although 36-inch diameter reflectors of good quality are readily available from surplus searchlights, this size was chosen as the most convenient for testing the procedure. Facilities are available at the fabricators for the production of such paraboloid mirrors up to 30 feet in diameter.

IX. FLUX DISTRIBUTION

Regardless of the radiation source, the focal area in image furnaces is not uniformly irradiated. The flux distribution usually can be illustrated by a bell-shaped curve with its maximum located at the center of the focal area (figure 16). When flux of such distribution impinges on a sample, a corresponding temperature distribution is generated. Thus, when a mechanical, physical, or chemical property of a sample is measured, it is possible to obtain only one value for the entire temperature range. Such a value has little, if any, definitive meaning so far as the temperature dependence of the property is concerned.

One possibility of overcoming this problem is to reduce, or preferably to completely eliminate the flux (temperature) differences through the use of optical elements. The most direct (and most difficult) approach consists of designing such a nonparaboloidal, compound curvature concentrator which delivers a uniform flux to the focal area. The only known effort in this direction is a small aluminum reflector built in the U. S. S. R.[8] It consists of aluminum strips arranged radially and narrowing down from the periphery to a circular piece at the center. It is claimed that this reflector gives a fairly uniform temperature distribution. No information, however, is available on how uniform the flux is and the amount of the loss in the maximum obtainable flux.

A second optical method[9] uses a kaleidoscope-type system placed in front of the sample. The system, consisting of a mirror-walled tube, receives the uneven flux from the reflector and, by multiple reflections, redistributes it to a well delineated even flux in the image area. The flux variations are less than ±5 per cent; and it is possible to adjust the size of the image, within limits, to particular requirements. The main disadvantage of this method is the fact that it greatly reduces the obtainable maximum flux, thus wiping out one of the most important advantages of image furnaces. In addition, approximately 50 percent of the total energy is lost in the redistributor.

A new method developed during the present investigation does not alter the uneven flux distribution, and thus does not reduce the maximum obtainable flux. Instead, this method makes it possible to interpret the measurements made with the uneven flux (temperature) distribution as if the results would have been obtained with a preselected narrow temperature range.

The method consists of measuring the property with the uneven but known temperature distribution. Following this, a second measurement is made after the temperature maximum has been altered by a preselected value. The changing of the temperature peak, followed by a measurement of the property, is repeated until the entire desired-temperature range is covered. From the results of these measurements the temperature dependence of the property is calculated.

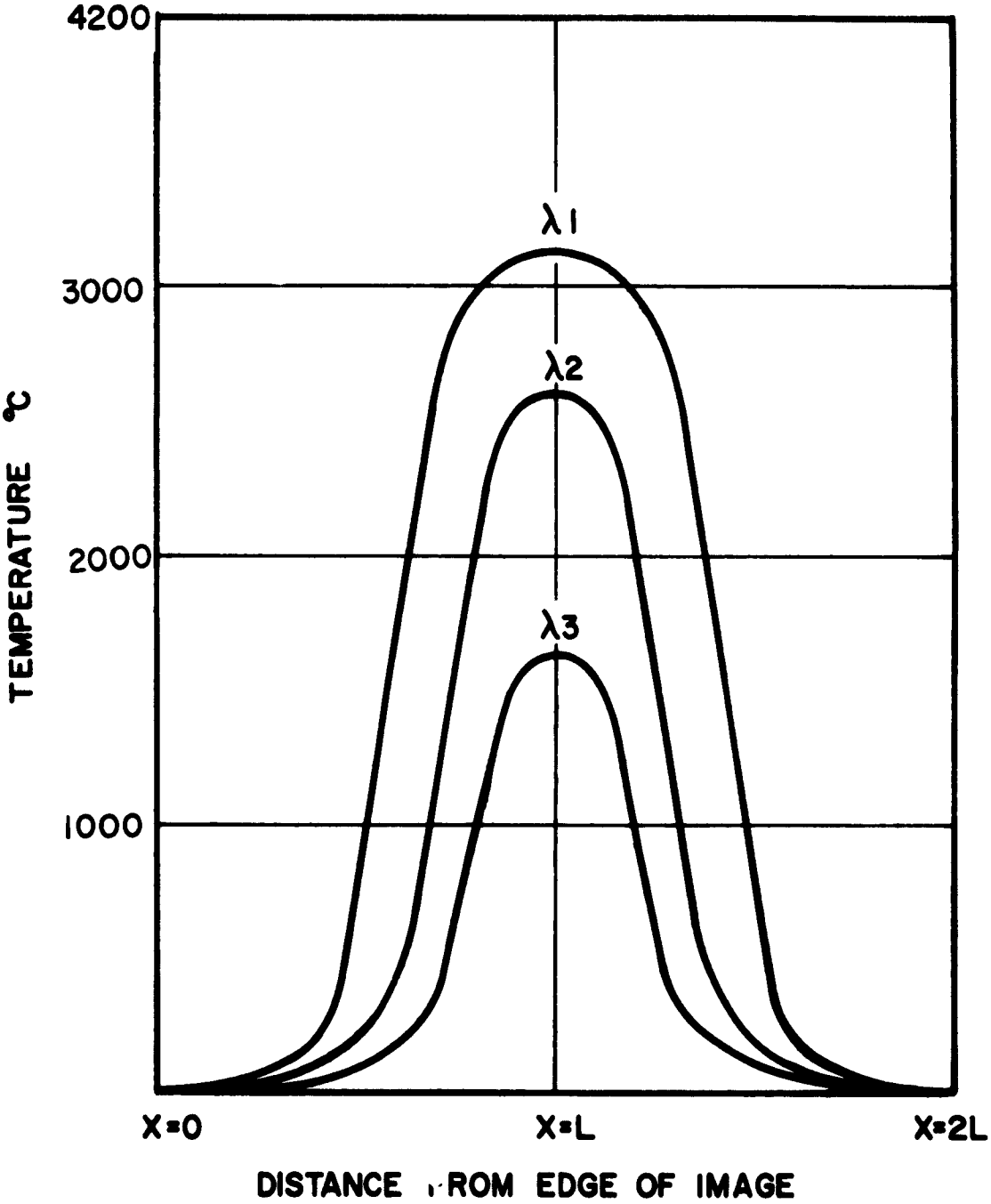

Figure 16 IMAGE TEMPERATURE DISTRIBUTION
63-2168

In an image furnace it is possible to change the maximum temperature by varying the position of the flux attenuator. The different temperature distributions as a function of the image diameter are illustrated in figure 16 where 2L is the diameter of the image. Let this family of curves be represented by

$$T = \phi(x, \lambda) \tag{1}$$

where x is the distance from the edge of the image and $\phi(x, \lambda)$ the temperature distribution.

The measured property per-unit-length at temperature T is denoted by $R(T)$. The total value of the property of the sample at a given temperature distribution is

$$\bar{R} = 2 \int_0^L R(T)\, dx \tag{2}$$

or

$$\bar{R} = 2 \int_0^L R\,|\phi(x, \lambda)|\, dx \tag{3}$$

This is an integral equation relating th desired function $R(T)$ to the temperature distribution $\phi(x, \lambda)$ and the measured total value of the property $\bar{R}(\lambda)$. Since the function $\phi(x, \lambda)$ is determined graphically, a numerical method of solution for $R(T)$ is proposed.

If it is desired to determine $R(T)$ for intervals of 300° C, at least 10 values are needed to cover the entire temperature range of 3000° C. This necessitates the measurement of 10 $\bar{R}(\lambda)$ values, one for each 300° C interval between temperature maxima. Ten temperature distribution curves, depicting $T = (x, \lambda)$ for the same intervals also are required. If $R(T)$ changes rapidly with temperature, the intervals may be decreased and the number of measurements increased in order to improve the accuracy of the method.

On the temperature-distribution curves, horizontal lines are drawn corresponding to the specified temperature brackets, e.g., at T_1 = 600° C, T_2 = 900° C ..... T_{10} = 3300° C. The intersection of each line with each $\phi(x,\lambda)$ curve determines a set of x and λ values. It then follows that the integral (3) can be approximated by the finite sum.

$$1/2\,\bar{R}(\lambda) = R(\bar{T}_1)(X_1 - X_0) + R(\bar{T}_2)(X_2 - X_1) \qquad (4)$$

$$+ \ldots\ldots R(\bar{T}_{10})(X_{10} - X_9)$$

or

$$\bar{R}(\lambda) = 2\sum_{i=1}^{10} R(\bar{T}_i)(X_i - X_{i-1}) \qquad (5)$$

Where $2\bar{T}_i = T_i + T_{i-1}$, $X_0 = 0$ and T_{10} is the maximum temperature obtained during the measurements. Consequently $X_{10} = L$.

From the 10 equations like (5), obtained for 10 different λ it is possible to determine the 10 unknown (T_i) values. The resultant values for $R(T)$ are plotted versus T, and a smooth curve is drawn from which values for R can be read off for each temperature interval, in this case 300° C.

In carrying out the experimental part of this method, it is important to determine accurately the temperature distribution of the sample placed in the image area as shown in figure 16. It is necessary not only to control the maximum temperature at the center but also the temperature at the coolest part of the sample. For this reason the sample holder designed for this method has liquid-cooled clamps in direct contact with the sample. The sample is a very thin rod and, accordingly, the only temperature distribution is lengthwise.

X. NEW SHAPE BLACKBODY

The high heat fluxes encountered in image furnaces are usually measured with calorimeters or with radiometers calibrated with calorimeters. Several water-cooled calorimeters have been designed which are suitable for use in image furnaces.[10] These calorimeters employ a spherical cavity as an artificial blackbody to absorb the incident radiation.

The problem of finding the optimum shape for an artificial blackbody has been investigated extensively. Buckley[11] studied the radiation from the inside of a circular cylinder. He derived an expression for the radiation from an annulus to any other annulus in a cylinder of infinite length taking into account multiple reflections. He then applied the same method to the case of a finite, uniformly heated cylinder and obtained an approximate solution. Finally, he adapted the method to the problem of a uniformly heated finite cylinder closed at one end, a shape which closely approximates some artificial blackbodies being used in optical pyrometry.

One of the most interesting results of his work is the relationship between cylinder length and orifice radius. This shows that if the emissivity of the cylinder wall is 0.75, a cylinder length/orifice-radius ratio of 3.8 gives radiation intensities within 1 percent of blackbody radiation. This ratio decreases rapidly as the emissivity of the wall increases, with the result that, for materials of high emissivity, the length of the cavity can be greatly reduced without reducing the orifice radius as well.

Gouffé compared the sphere, the cylinder, and the conc in his search for the optimum artificial blackbody shape.[12] He based his comparison on the value L/R, where L is the length of the blackbody and R is the radius of its orifice. From these data, he calculated the total surface area of the cavity S and the surface area of the orifice s. The ratio s/S then expressed the relative value of the cavity as a radiant-energy trap. It should be pointed out that in his calculation, S includes the area of the orifice s, which is not an absorbing surface. A more exact expression for the evaluation of the cavity would be s/S-s. The shapes considered by Gouffé are shown in figure 17 a, b, c.

During the present investigation, a new shape for artificial blackbodies was conceived, consisting of a truncated right cone with the smaller end as the orifice. The bottom of the cavity is a right circular cone (figure 17 d). In a cavity of this shape, only a very small fraction of the total area "sees" the orifice perpendicularly and, accordingly, losses due to reradiation are low.

Gouffé's method of evaluation has been applied to this shape. The results, together with Gouffé's data for the shapes he has considered are presented in table I.

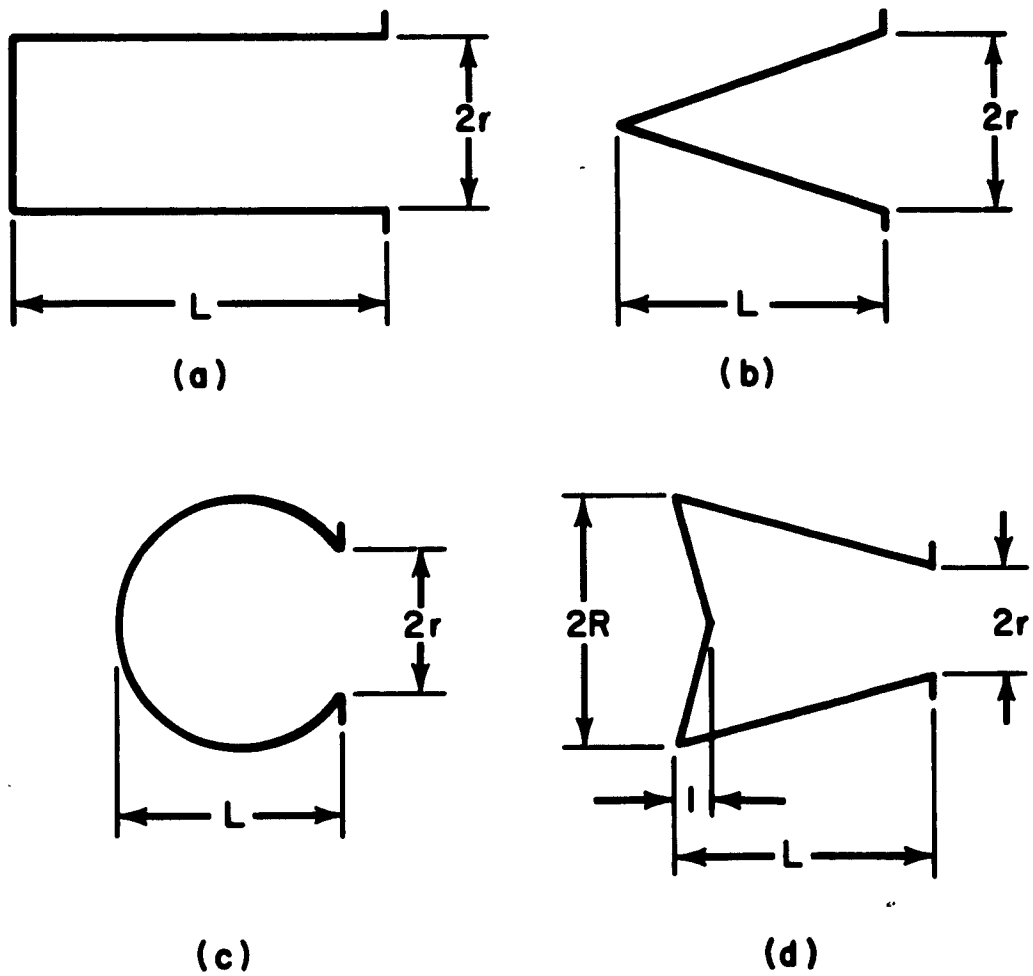

Figure 17 ARTIFICIAL BLACKBODY SHAPES
60-2633

TABLE I

COMPARISON OF ARTIFICIAL BLACKBODY SHAPES

L/R	s/S				s/S - s/S_o †		
	Sphere*	Cylinder*	Cone*	Double Cone**	Cylinder*	Cone*	Double Cone**
1	0.500	0.250	0.415	0.175	-0.250	-0.085	-0.325
2	0.200	0.167	0.309	0.094	-0.033	+0.109	-0.106
3	0.100	0.125	0.241	0.059	+0.025	+-.141	-0.041
4	0.059	0.100	0.195	0.041	+0.041	+0.136	-0.018
5	0.039	0.083	0.164	0.030	+0.044	+0.125	-0.009
6	0.016	0.056	0.111	0.015	+0.040	+0.095	-0.001

*Shapes Considered by Gouffe
**Shape Proposed by Present Investigation
† Comparison of Shapes with Sphere (s/S_o)

From the table, it can be seen that if the L/R ratio is greater than 2, both the cylinder and the cone are inferior to the sphere as indicated by the s/S value. The double cone shape, however, results in an s/S value which is more favorable than that for the sphere, even for L/R ratios as high as 8. Such a high L/R ratio is required only if the emissivity of the wall is as low as 0.25, an unlikely choice for the cavity material.

The s/S ratio, however, does not express perfectly how closely a cavity approximates the radiation characteristics of a blackbody. The effect of multiple reflections must be considered in order to determine what fraction of the radiation entering the cavity will escape from it after many relections from its walls. Therefore, using an analytical approach, a set of integral equations was developed. The equations determine the effective emissivity for an almost blackbody by considering every point of the cavity as both a receiver and an emitter of radiation. The body under consideration is depicted in figure 18.

The letters S_o, S_i, and S_p, respectively, denote the following surfaces of the body:

S_o - outer conical surface.

S_i - inner conical surface.

S_p - plane surface of aperture.

The equations for the three surfaces are given as follows:

$$S_o: \quad x^2 + y^2 = a^2 z^2 \quad (a - \text{fixed})$$

$$h \geq z \geq h_o \qquad (h_o - \text{fixed}) \tag{6}$$

$$S_i: \quad x^2 + y^2 = b^2 (z - h_1)^2$$

$$h \geq z \geq h_1$$

$$b = ah/(h - h_1) \tag{7}$$

$$S_p: \quad z = h_o$$

$$x^2 + y^2 \leq r_o^2 = a^2 h_o^2 \quad (r_o - \text{fixed}) \tag{8}$$

These equations are transformed into cylindical coordinates with the parameters ρ and θ.

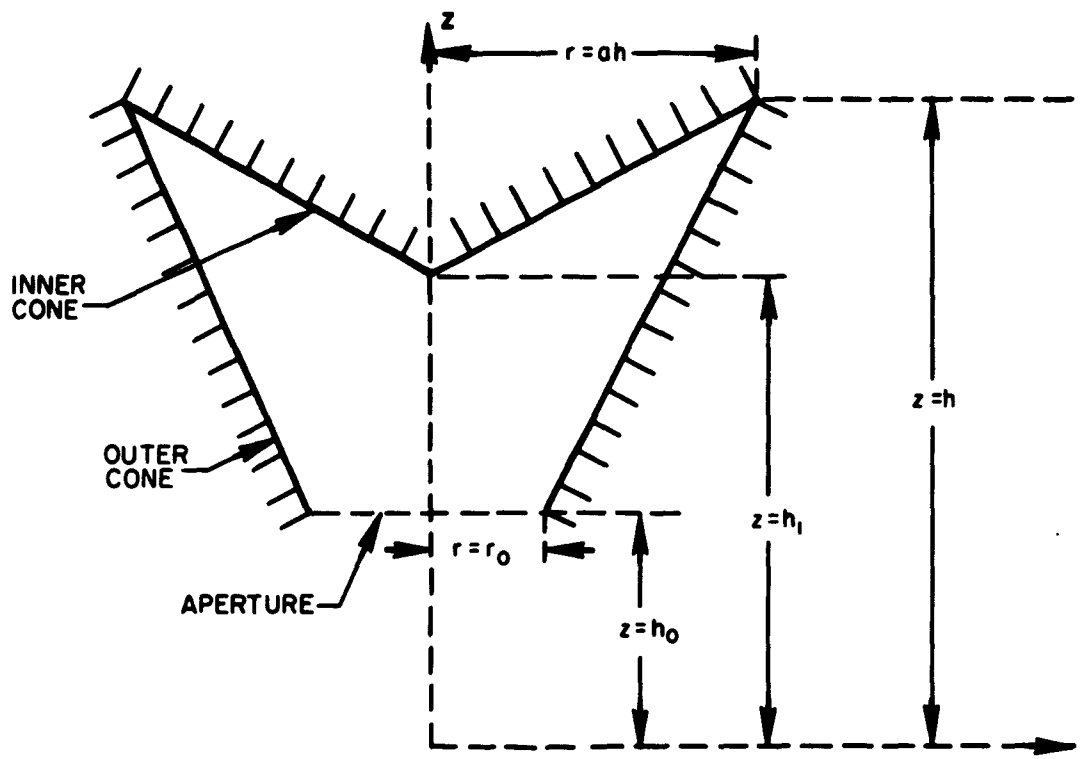

Figure 18 NEW SHAPE BLACKBODY
63-2344

A source of light is located on the axis of the body in such a manner that the cone of light formed by the aperture has a semivertical angle of 70 degrees. The problem then is to determine the ratio of the energy which comes out of the body through S_p to the energy entering it, taking into consideration the multiple reflections in the cavity.

The assumption is made that the walls of the cavity reflect perfectly diffusely (i.e., all surfaces have constant radiance); then[13]

$$\pi H(\rho',\theta') = \int_S \bar{H}(\rho,\theta)\, r(\rho,\theta)(-\vec{R}\cdot\vec{n})(\vec{R}\cdot\vec{n}')\,\frac{dA}{\vec{R}^4}$$

$$+ \int_s H(\rho,\theta)\, r(\rho,\theta)(-\vec{R}\cdot\vec{n})(\vec{R}\cdot\vec{n})\,\frac{dA}{\vec{R}^4} \qquad (9)$$

where

$\bar{H}(\rho,\theta)$ = irradiance at point (ρ,θ) due to the primary beam without any reflections,

$H(\rho',\theta')$ = irradiance at point (ρ',θ') caused by the reflected flux,

$r(\rho,\theta)$ = total reflectance at point (ρ,θ),

$\vec{n}$ = unit normal at point (ρ,θ) of surface,

$\vec{n}'$ = unit normal at point (ρ',θ') of surface,

$\vec{R}$ = position vector from point (ρ,θ) to point (ρ',θ').

The reflectivity $r(\rho,\theta)$ is zero on the aperture S_p and is constant on surfaces S_o and S_i.

As the cavity is made up from the three different surfaces S_o, S_i, and S_p, the kernel function $K(\rho,\theta,\rho',\theta') = (-\vec{R}\cdot\vec{n})(\vec{R}\cdot\vec{n}')/\vec{R}^4$, will have different representations according to which pair of surfaces the points (ρ,θ) and (ρ',θ') correspond to.

This expression assumes that any point of the surface can be seen from any other point on the surface. This, however, is not the case. Accordingly, the equation must be first integrated over the whole surface and then the shadowed surface, i.e., that portion of the surface which cannot be seen from the point (ρ',θ') must be subtracted from the integral. Because of the axial symmetry, $H(\rho',\theta')$ is independent of θ and thus can be integrated out of the kernels. The following three sets of equations express the solution of the problem as given for both the shadowed and unshadowed portions of the cavity.

$$\pi r^{-1} H_o(\rho') = \int_{ah_o}^{ah} \left\{H_o(\rho) + \bar{H}_o(\rho)\right\} K'_{oo}\, d\rho + \int_{o}^{ah} \left\{H_i(\rho) + \bar{H}(\rho)\right\} K'_{oi}\, d\rho \qquad (10)$$

(Unshadowed Case)

where K'_{oi} denotes the kernel function K when point (ρ') is an element of S_o [i.e., $(\rho') \epsilon S_o$ and $(\rho) \epsilon S_i$ and similarly for the other K's].

$$\pi r^{-1} H_o(\rho') = \int_{ah_o}^{ah} \left\{H_o(\rho) + \bar{H}_o(\rho)\right\} \left\{K'_{oo} - K''_{oo}\right\} d\rho + \int_{o}^{ah} \left\{H_i(\rho) + \bar{H}_i(\rho)\right\} K''_{oi}\, d\rho \qquad (11)$$

(Shadowed Region)

$$\pi r^{-1} H_i(\rho') = \int_{ah_o}^{ah} \left\{H_o(\rho) + \bar{H}_o(\rho)\right\} \left\{K'_{io} + K''_{io} + K'''_{io} + K''''_{io}\right\} d\rho \qquad (12)$$

$$\pi r^{-1} H_P(\rho') = \int_{ah_o}^{ah} \left\{H_o(\rho) + \bar{H}_o(\rho)\right\} K'_{Po}\, d\rho + \int_{o}^{ah} \left\{H_i(\rho) + \bar{H}_i(\rho)\right\} K_{Pi}\, d\rho \qquad (13)$$

The set of expressions were programmed for the Philco S-2000 high-speed computer. As a check of the theory and the correctness of the programming, numerical data were substituted for the hypothetical case of a blackbody with a wall reflectivity of unity. Since, in this case, the radiation incident in the blackbody is completely reflected whenever it hits the walls after multiple reflections,

the same flux should emerge from the blackbody as entered. However, the results of the numerical computation indicated that the intensity at the intersections of the inner and outer cones became unbounded for the test case of reflectivity equal to unity. Theoretical considerations show that this can physically happen, and when it does occur the computer cannot compute the test case because of the singularity. The difficulty was resolved by assuming that the reflectivity of the wall approaches, but does not equal, unity. The completed program was then checked and found to be satisfactory. Following this, the program was applied to the computation of several cases with various parameter combinations. The emissivity of the cavity wall was taken alternately as 0.25, 0.50, and 0.75. For each of these respective cases, the cavity length-orifice radius ratio (L/R) was taken as 2, 3, and 4. The results of these calculations are presented in figure 19 together with the values for a cylindrical cavity as calculated by Buckley.[11] The marked points are values obtained in the computation. As expected for low wall emissivity (0.25) and low L/R value (2), the improvement in effective emissivity due to the new shape is very high going from 0.67 to 0.89. As the L/R value increases, the relative improvement decreases; but it remains significant, even for L/R = 4. The improvement is smaller for 0.50 wall emissivity, and it shows the trend of decreasing with increasing L/R value. As the emissivity increases further, the improvement becomes even smaller. This is to be expected, since the closer the maximum is approached the more difficult it becomes to improve the effective emissivity. But, even when the wall emissivity is 0.75, a value which can easily be obtained in practice, the effective emissivity of the new shape is higher than that of the cylinder for the calculated L/R values.

In a second group of computations, the wall emissivity was held constant at 0.90 and the L/R ratio at 1.5. The cone angle was varied from 45 to 55 degrees. The results, as presented in figure 20, show that the effective emissivity increases with decreasing cone angle. The emissivity for a 45-degree cone angle with the above parameters is 0.9957, a very good approximation of an ideal blackbody.

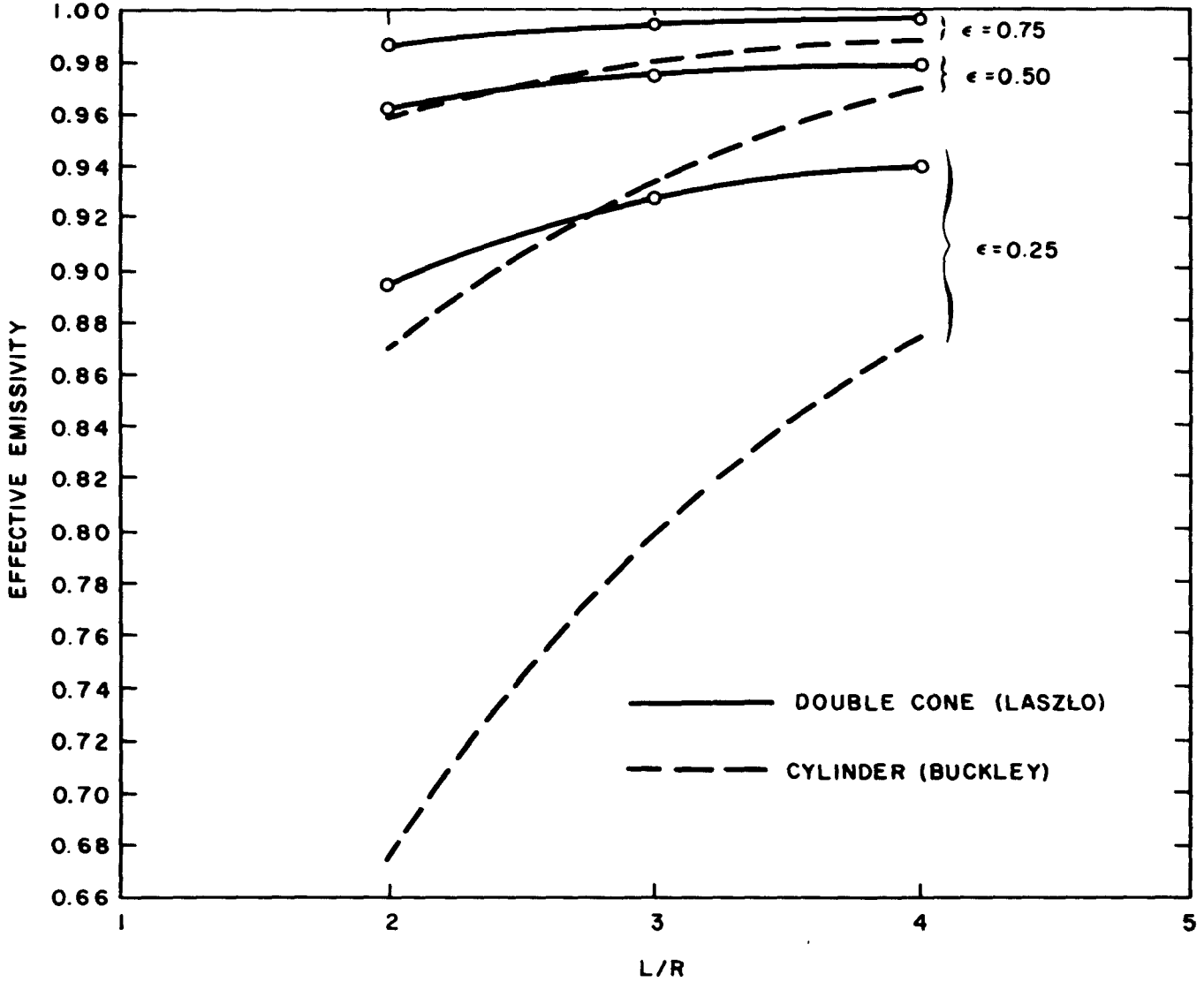

Figure 19 COMPARISON OF THE EFFECTIVE EMISSIVITY OF THE CYLINDER WITH THAT OF THE NEW SHAPE BLACKBODY
62-3770A

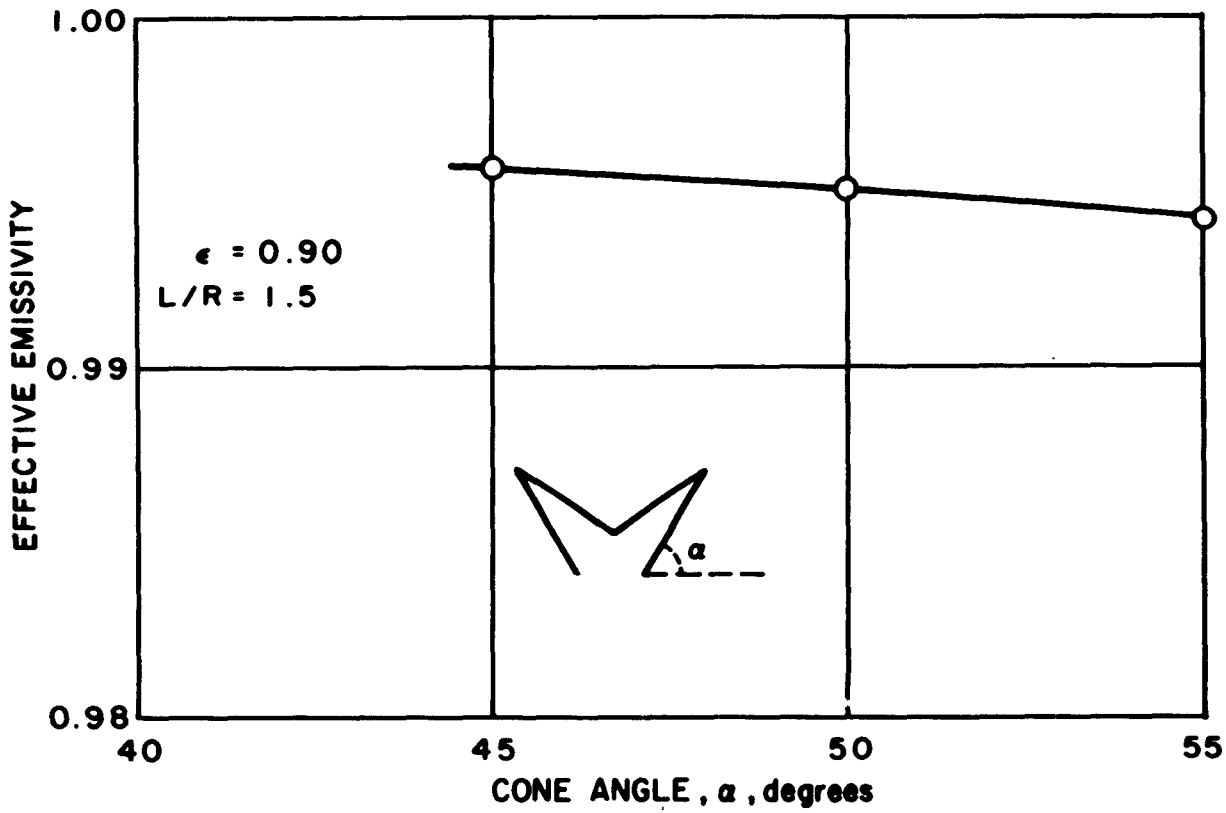

Figure 20 CONE ANGLE VERSUS EFFECTIVE EMISSIVITY OF THE NEW SHAPE BLACKBODY
62-3771

XI. CALORIMETRIC AND RADIOMETRIC MEASUREMENTS

A. CALORIMETRY

A water-cooled calorimeter has been constructed using an adiabatically installed absorbing cavity of the new shape. The calorimeter is mounted in the focal area of the solar furnace, and the concentrated radiant flux enters through a well-defined orifice. The radiant energy is absorbed by the cavity walls, and the heat thus generated is transmitted to distilled water passing through the water-jacket of the cavity at a controlled and measured rate of flow. The resultant water temperature rise is measured with differential thermopiles. The mass of the water and the elapsed time is also measured. From these data, the total amount of radiant energy entering the cavity can be calculated. A block diagram of the experimental set-up is shown in figure 21.

The normal incident solar radiation is concurrently measured with an Eppley normal-incidence pyrheliometer mounted directly on the solar furnace parallel with its optical axis. The time and length of each calorimetric run is recorded on the normal-incidence chart, thus synchronizing the two measurements. From these data, the radiant-energy flux-per-unit normal-incidence solar radiation (Ly/min) is calculated. Several hundred such flux measurements have been made in the 60-inch solar furnace. Some of the results of these measurements are presented in table II. In this table, the flux-controlling screen position is indicated on an arbitrary linear scale. At the maximum flux the deviation from the average is ± 3.7 percent. The average flux values have been plotted against the screen position in figure 22.

The shape of the resultant curve is seen to be suggestive of that of a parabola. Accordingly, the curve was plotted using a parabolic scale on the ordinate. At the same time the abscissa linear scale of the flux-controlling screen was changed to the more meaningful effective rim angle of the mirror. The result of this plot is shown as the lower curve in figure 23 for unit Ly/min normal incidence.

These results prove the direct relationship between normal incidence solar radiation intensity and the concentrated flux at the image area. Thus, by measuring the normal incidence solar radiation the average flux value at the focal area can be obtained through the use of the above correlation. The flux is continuously variable from 35 to approximately 360 cal/cm^2-sec depending on the normal-incidence solar radiation and on the position of the flux-control screen. Because of this well-defined correlation, the solar furnace can be used as a high-intensity radiation standard with a maximum average flux of 360 cal/cm^2-sec ± 3.7 percent, a value superior to any thermal radiation standard known to be available.

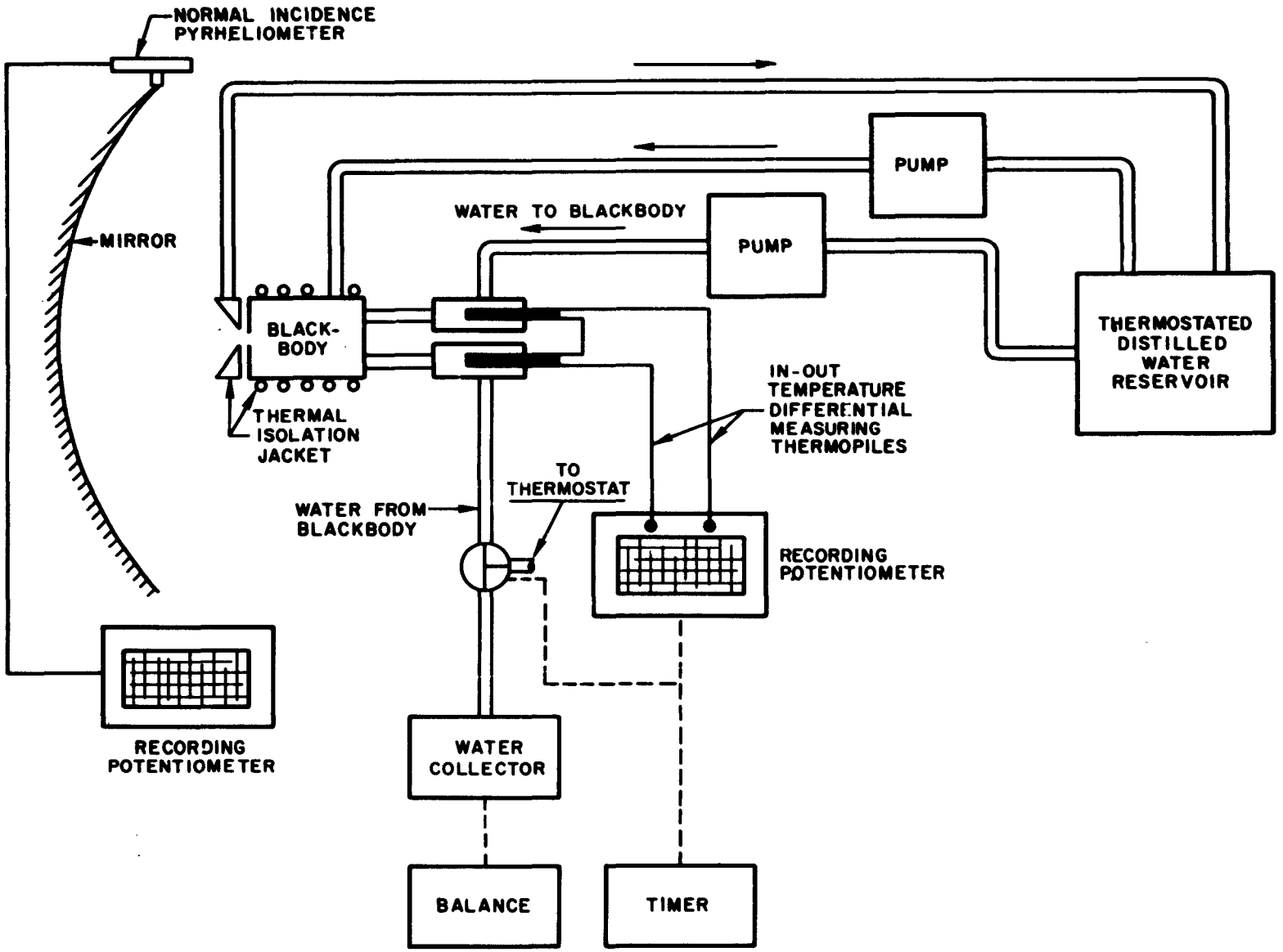

Figure 21 BLOCK DIAGRAM OF CALORIMETRIC MEASUREMENT SYSTEM
61-3851

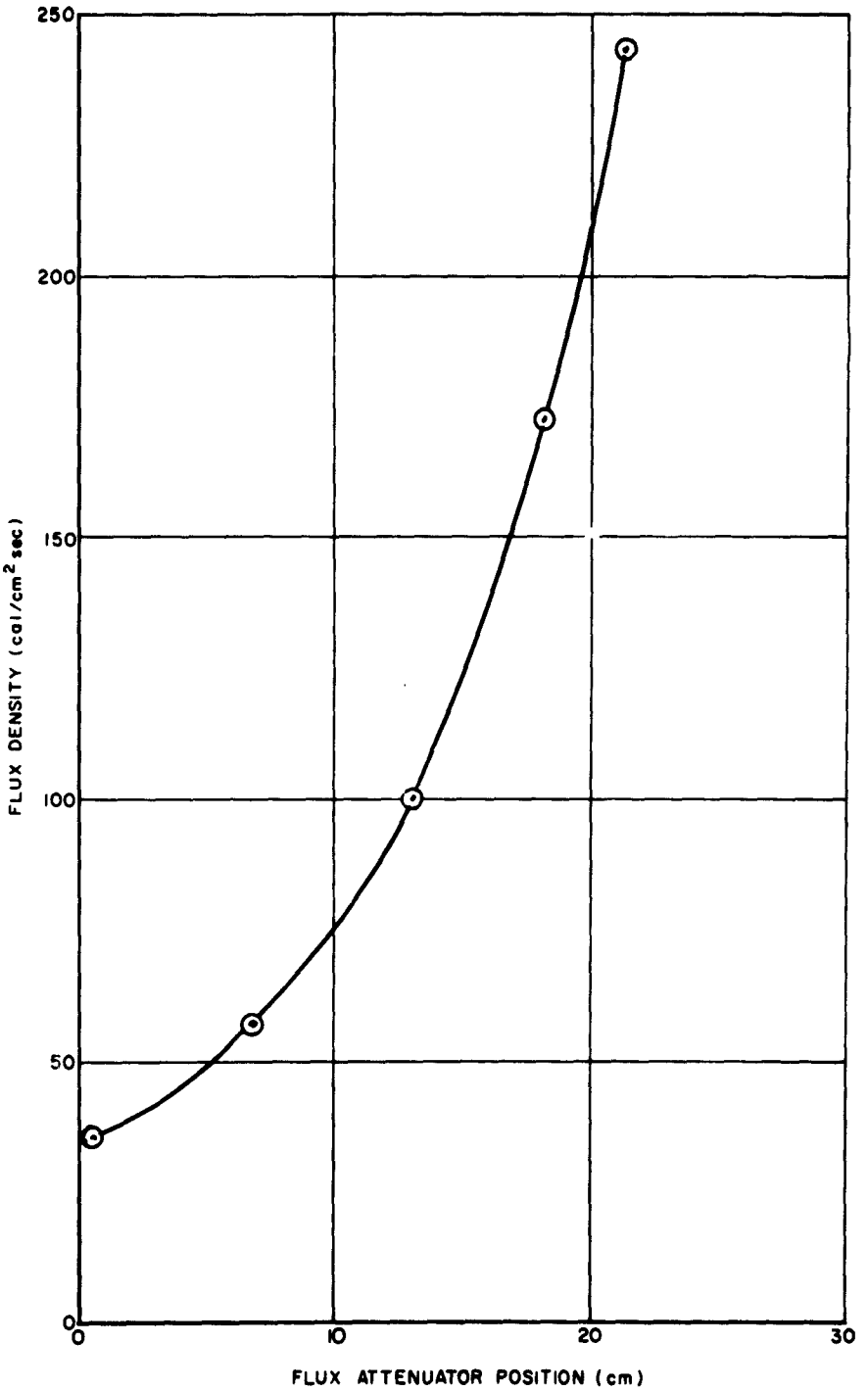

Figure 22 FLUX VERSUS ATTENUATOR POSITION IN THE SOLAR FURNACE
61-5017

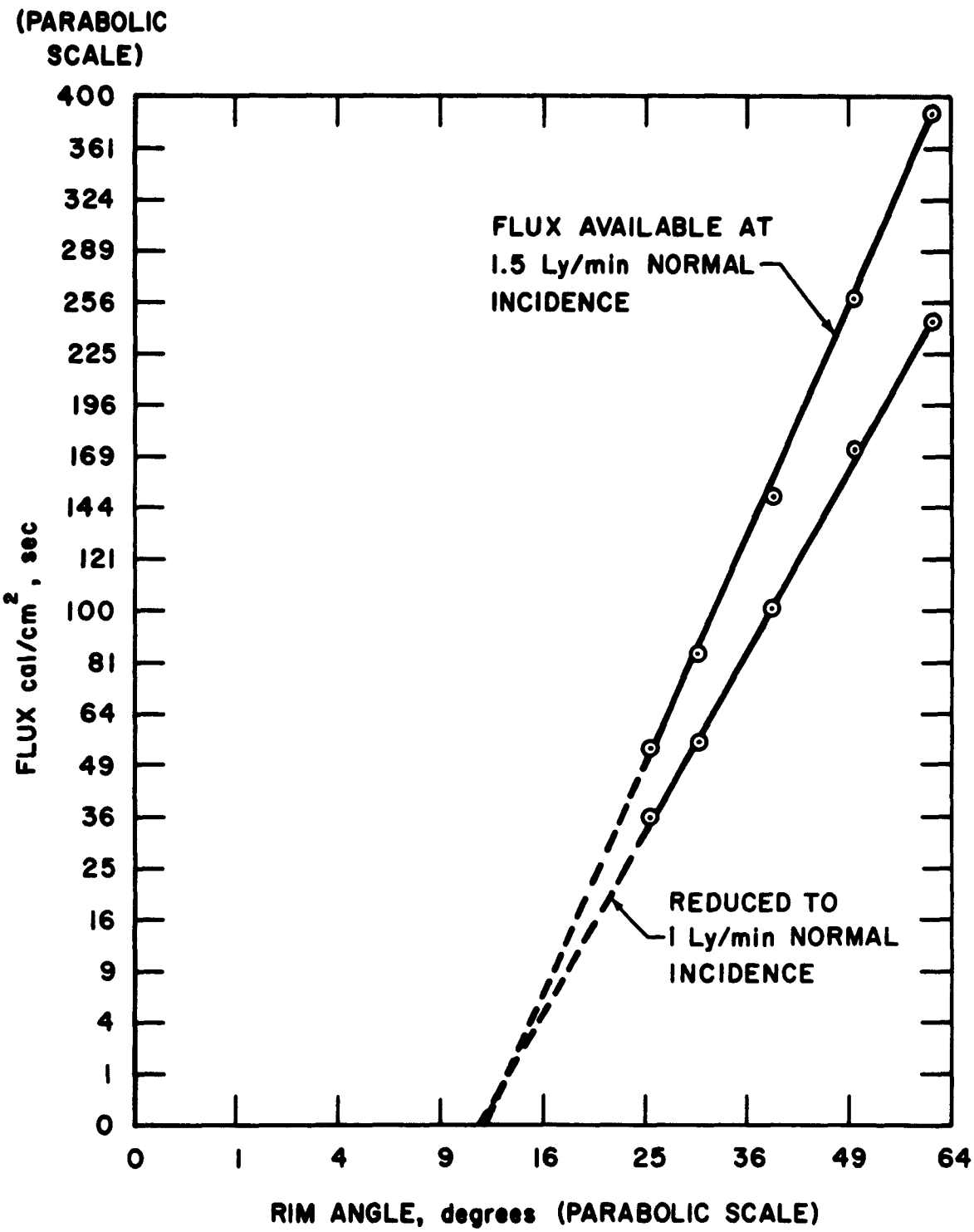

Figure 23 FLUX VERSUS RIM ANGLE
61-3893

TABLE II

FLUX VERSUS SCREEN POSITION MEASURED IN THE AVCO RAD 60-INCH SOLAR FURNACE (NORMALIZED TO 1 LY/MIN NORMAL-INCIDENCE SOLAR RADIATION)

Screen Position	0.5 cm	6.5 cm	12.8 cm	18.1 cm	Full Out
Flux values (cal/cm^2-sec)	34.08	53.91	96.46	168.59	235.94
	34.16	54.44	97.27	168.92	237.23
	34.18	54.50	97.45	169.47	238.10
	34.35	55.30	97.59	169.65	239.66
	34.59	55.51	97.69	170.30	240.42
	34.62	55.63	97.78	170.46	241.28
	34.67	55.66	98.35	170.51	241.33
	35.00	55.69	98.51	171.04	241.50
	35.02	55.83	98.90	171.43	241.68
	35.05	55.94	99.06	171.43	241.99
	35.14	55.95	99.09	171.56	242.46
	35.27	56.21	99.55	171.59	242.74
	35.31	56.36	99.62	171.79	243.31
	35.48	56.44	99.99	171.98	243.42
	35.49	56.53	100.18	172.39	244.96
	35.59	56.56	100.76	173.03	245.12
	35.61	56.61	102.23	173.04	245.13
	35.69	56.84	102.27	173.24	245.60
	35.85	56.96	102.33	173.49	246.31
	35.87	57.20	103.07	173.76	246.45
	35.90	57.26	103.12	174.47	247.21
	35.93	57.34	103.15	174.61	247.46
	35.93	57.41	103.16	174.63	247.63
	35.96	59.25	103.24	174.88	247.72
	36.02	59.48	103.44	175.49	248.01
	36.07	59.90	104.07	175.70	248.16
	36.16	60.32	104.35	175.71	248.72
	36.18	60.75	105.88	177.92	249.09
	36.44	61.02		178.57	249.49
	36.48	61.72		179.21	249.74
	36.69				251.36
	36.81				251.51
	36.82				251.83
	37.07				252.42
	37.08				253.86
	37.13				
Average flux value	35.67	57.08	100.63	172.96	245.40
Deviation from the average (%)	±4.4%	±6.8%	±4.6%	±3.1%	±3.7%
Median flux value	35.85	56.55	100.09	172.71	245.60
Deviation from the median (%)	±4.2%	±6.9%	±4.8%	±3.1%	±3.7%

The results of the flux measurements have been scrutinized as to the possible effects of experimental conditions (table III). Flux values measured at 25-degree, 24-minute rim-angle screen position are arranged in calendaric order. The measured flux appears to be independent of the variations in ambient temperature, large though they were. During this time, the mirror of the solar furnace was frequently exposed to outdoor corrosive agents and was washed every two or three weeks. No decline in flux values indicative of deterioration of the mirror surface was apparent.

Table IV represents flux values measured at the effective 61-degree, 22-minute rim-angle screen position at various solar incidences. From these data it is apparent that the flux values, reduced to 1 Ly/min normal incident are independent of the actual value of the normal incidence. In table V the results of flux measurements taken at 49-degree, 46-minute rim-angle screen positions are shown, together with the various waterflow rates of the calorimeter. As expected, changes in waterflow rate do not affect the results of the calorimeter measurements.

These considerations appear to prove that the flux in a particular solar furnace depends only on the normal-incidence solar radiation and the position of the flux-control mechanism (or active rim angle of the mirror). The maximum obtainable flux is defined by the normal-incidence solar radiation at the time of the experiment. Any flux value below this can be obtained by the adjustment of the flux-control mechanism.

Once the correlation between normal-incidence solar radiation and the concentrated flux has been determined for a particular furnace, it can be used to produce a flux of known value up to the maximum obtainable. The reduced flux values, as presented in table II and figure 22 are multiplied by the actual value of normal-incidence solar radiation. Thus, a correlation is obtained between the actual flux at the focal zone and the position of the flux attenuator. An example of this is presented in figure 23, where the upper line represents the actual flux values for a normal incidence of 1.5 Ly/min, the highest value measured thus far at the furnace location. This same procedure can be used for any other normal incidence of solar radiation.

It is interesting to note that the two lines intersect the abscissa at the same point. This point represents that rim-angle mirror section which produces zero flux (11 degrees, 58.8 minutes). Accordingly, it can be assumed that all causes of fixed flux losses, such as the shadow cast by the sample holder, mirror cut-out, and so forth, are contained in a paraboloid of 11-degree, 58.8-minute rim angle. This method can be used for the experimental determination of such losses of image furnaces.

TABLE III

FLUX MEASURED AT DIFFERENT TIMES OF THE YEAR

Flux* (cal/cm^2-sec)	Date	Flux (cal/cm^2-sec)	Date
34.08	3 Oct	35.85	18 Nov
34.16	4 Oct	35.87	5 Oct
34.18	24 Aug	35.90	15 July
34.35	4 Oct	35.93	18 Nov
34.59	3 Oct	35.93	18 Nov
34.62	24 Aug	35.96	5 Oct
34.67	24 Aug	36.02	15 July
35.00	4 Oct	36.07	15 July
35.02	7 Oct	36.11	12 Jan
35.05	18 Nov	36.16	7 Oct
35.14	18 Nov	36.18	18 Nov
35.27	7 Oct	36.44	15 July
35.31	7 Oct	36.48	15 July
35.48	12 Jan	36.69	5 Dec
35.49	7 Oct	36.81	26 Sept
35.59	3 Oct	36.82	26 Sept
35.61	12 Jan	37.07	26 Sept
35.69	3 Oct	37.08	5 Dec
		37.13	5 Dec

*Flux values reduced to 1 Ly/min normal incidence. Measurement taken with a 25-degree, 24-foot rim angle.

TABLE IV

FLUX MEASURED AT VARIOUS NORMAL SOLAR INCIDENCE VALUES

Flux (cal/cm-sec)	Normal Incidence (Ly/min)	Flux (cal/cm^2-sec)	Normal Incidence (Ly/min)
235.94	1.33	245.60	0.98
237.23	1.31	246.31	1.07
238.10	1.35	246.45	1.13
239.66	1.13	247.21	1.12
240.42	1.30	247.46	0.90
241.28	1.27	247.63	0.94
241.33	1.30	247.72	0.92
241.50	1.30	248.01	1.30
241.68	1.02	248.16	1.10
241.99	1.27	248.72	1.08
242.46	1.14	249 09	1.29
242.74	1.14	249.49	1.27
243.31	1.14	249.74	0.85
243.42	1.28	251.36	1.26
244.96	1.29	251.51	1.26
245.12	1.27	251.83	1.08
245.13	1.12	252.42	1.26
		253.86	0.86

*Flux values reduced to 1 Ly/min normal incidence. Measurements taken with a 61-degree, 22-foot rim angle.

TABLE V

FLUX MEASURED AT VARIOUS WATER FLOW RATES

Flux* (cal/cm^2-sec)	Water Flow Grams/min	Flux (cal/cm^2-sec)	Water Flow Grams/min
168.59	571.1	173.03	447.2
168.92	470.4	173.04	548.4
169.47	473.6	173.24	470.0
169.65	561.6	173.49	462.4
170.30	433.7	173.76	462.7
170.46	448.4	174.47	549.5
170.51	559.8	174.61	549.3
171.04	561.6	174.63	468.5
171.43	462.0	174.88	558.2
171.43	440.1	175.49	555.1
171.56	440.4	175.70	467.8
171.59	402.5	175.71	566.2
171.79	470.3	177.92	550.1
171.98	461.7	178.57	555.5
172.39	462.8	179.21	559.9

*Flux values reduced to 1 Ly/min normal incidence. Measurements taken with a 49-degree, 46-foot rim angle.

B. RADIOMETRY

Calorimetric measurements yield an average value for the flux across the entire orifice. The flux, however, is not uniform; it shows a very sharp peak at the center of the image. In order to measure the flux distribution with fine resolution, a radiometer is needed which has a small sensing area, and which can be moved across the hot zone without damage. The only fast-response instrument available with the necessary characteristics for the measurement of high-heat fluxes encountered in solar furnaces is the modified Gardon radiometer.[14] It consists of a water-cooled, copper-constantan thermocouple, the constantan being in the form of a thin, circular foil. This instrument has a fast response (60 percent of signal reached in 0.02 sec) and a fine resolution (sensing disc diameter is 0.899 mm). However, the carbon camphor-soot coating of the disc, as supplied by the manufacturer of the instrument, has two major deficiencies: (1) its emissivity is not constant above 270° C, and (2) it tends to burn off in the presence of oxygen when exposed to high heat fluxes.

It was proposed that a solution to this problem possibly can be found by replacing the carbon coating with one of magnesium oxide and, therefore, an experimental program was begun to verify this. While the emissivity of MgO is much lower than that of carbon, the coating is very stable for all flux values under consideration, even in oxidizing atmospheres. It has been reported[15] that the reflectivity of MgO changes with time. This aging effect was attributed to the decomposition of magnesium nitride traces under the influences of ultraviolet radiation. It was assumed that the traces of magnesium nitride are formed when MgO is deposited by burning magnesium in air. This assumption was proved by the generation of ammonia gas on contact of the product of combustion with water. However, the nitride was converted to the oxide shortly after the freshly coated radiometer was exposed to the high-heat flux in the solar furnace. This was observed as the sensitivity of a freshly coated radiometer decreased during the first few minutes of exposure but became stable after approximately 10 minutes. Accordingly, before a freshly coated radiometer was used for measurements, it was "baked out" at maximum heat flux for 10 minutes. Another advantage of the MgO coating over the carbon coating is the fact that an old, contaminated coating can be easily removed with water and a new coating quickly applied.

Although the sensitivity of the radiometer can be calculated from the dimensions of the sensing disc,[16] the instrument has to be calibrated for precise measurements. The flux in the image area is known from the calorimetric flux measurements as outlined in section A above. These values, however, represent an average across the entire image as the orifice of the calorimeter cavity is approximately the same size as the image. The diameter of the radiometer sensing disc is approximately one-tenth that of the image diameter. Therefore, any single reading of the radiometer cannot be equated with the average flux value determined calorimetrically.

This difficulty was overcome by the following method: the radiometer was coated with MgO and baked out. The instrument was then positioned at the exact center of the focal area and moved across the image along the horizontal axis. Its emf output was recorded and its position relative to the center of the image was indicated on the emf record chart. Five crossings were made for each reading and the average values were used in the calculation. Five to 10 readings were taken for each coating in order to establish the stability of the sensitivity.

A typical record thus obtained is the bellshaped curve on figure 24. In this graph the abscissa is the image radius in cm with the 0 at the center of the image, and the ordinate is the radiometer emf output. The problem now is reduced to finding the flux equivalent of the recorded emf values.

Superimposed on the bellshaped curve is a rectangle (striations running upward). This rectangle represents the average flux over the entire image area as measured by the calorimetric method (Section XI. A). The abscissa has the same value for both curves, but for the calorimetric record the ordinate represents flux and its scale is known. By rotating both curve and rectangle around the 0 abscissa axis, two volumes are defined. Both volumes represent the total energy content of the image area and are, therefore, equal. For the rectangle, both ordinate and abscissa are known numerically, and from these data the volume is calculated.

$$V_{cy} = \pi r^2 h \tag{14}$$

where

r = the radius of the focus.
h = the flux density

For the radiometer output curve only the abscissa is known numerically; the ordinate in term of flux is unknown. The numerical value of the volume defined by rotating the curve can be obtained, however, from the graph by the trapezoidal method

$$V_{RC} = 2\pi \sum_{o}^{r} (rh)_{av} \Delta r \tag{15}$$

where

$$(rh)_{av} = \frac{(r_n h_n + r_{n+1} h_{n+1})}{2}$$

$$\Delta r = r_{n+1} - r_n$$

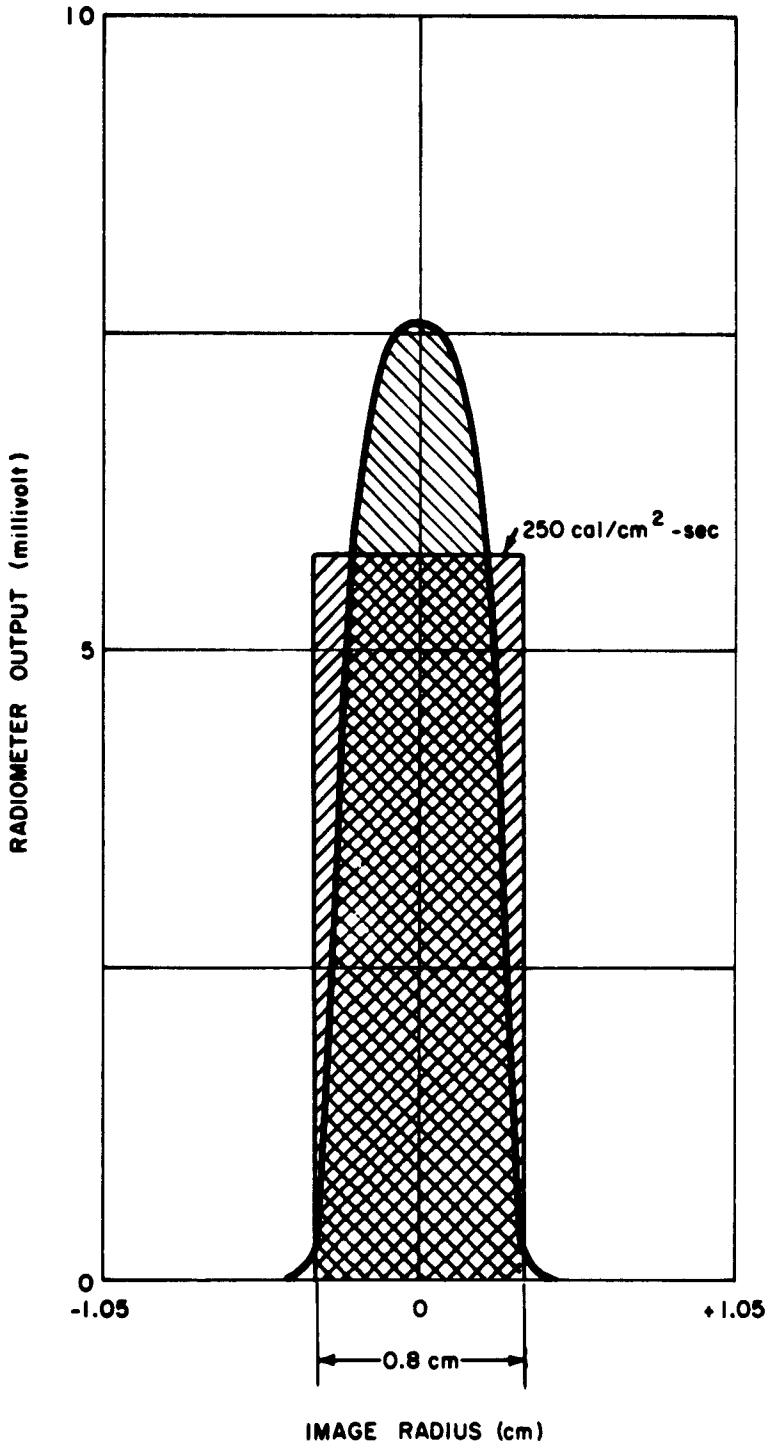

Figure 24 CALIBRATION OF RADIOMETER
61-488

r is the radius of the focal area, divided into n increments, selected to achieve the desired precision,

h is the ordinate value for each increment of r in terms of emf.

By equating the two volumes, a scale factor k is calculated:

$$k = \frac{\pi r^2 h}{2\pi \sum_{o}^{r} (rh)_{av} \Delta r} \tag{16}$$

If Y is the height read from the graph in terms of emf, then kY_{max} transforms the emf ordinate value into flux. The emf/flux ratio in turn is the sensitivity of the radiometer.

Measurements were performed in order to determine whether the sensitivity of the radiometer is constant under all flux conditions obtainable in the solar furnace. First, the radiometer was placed at the center of the focal area and its output was recorded while the flux-control screen was moved from minimum to maximum flux position. The radiometer output is shown in figure 25. From the principle of flux modulation with the screen, the absolute flux value at any screen position is a function of the normal incidence solar radiation, and the ratio of flux values at given screen positions is constant.

The radiometer output was recorded at five arbitrarily selected screen positions, and the ratio of output at four positions was taken with respect to one screen position (0.5 cm). More than 100 such flux measurements were made using 10 different MgO coatings on the radiometer. The results of the ratio computations are summarized in table VI for a wide variance of normal solar-incidence values. These results prove that for any MgO coating the ratio of emf output for a particular flux value to a preselected flux value is constant and independent of the normal-incidence solar radiation. This can be so only if the sensitivity of the instrument is constant within the flux values obtained in the solar furnace.

In a second group of measurements, efforts were made in order to establish a correlation between MgO coating thickness and sensitivity. Should such a correlation exist, the sensitivity determination could be reduced to a single measurement of coating thickness. A reference line was engraved on the housing of the radiometer adjacent to the sensing disc. The distance of the uncoated disc from the reference line was measured microscopically. The disc was then coated with MgO, and the distance of the coating surface from the reference line was measured.

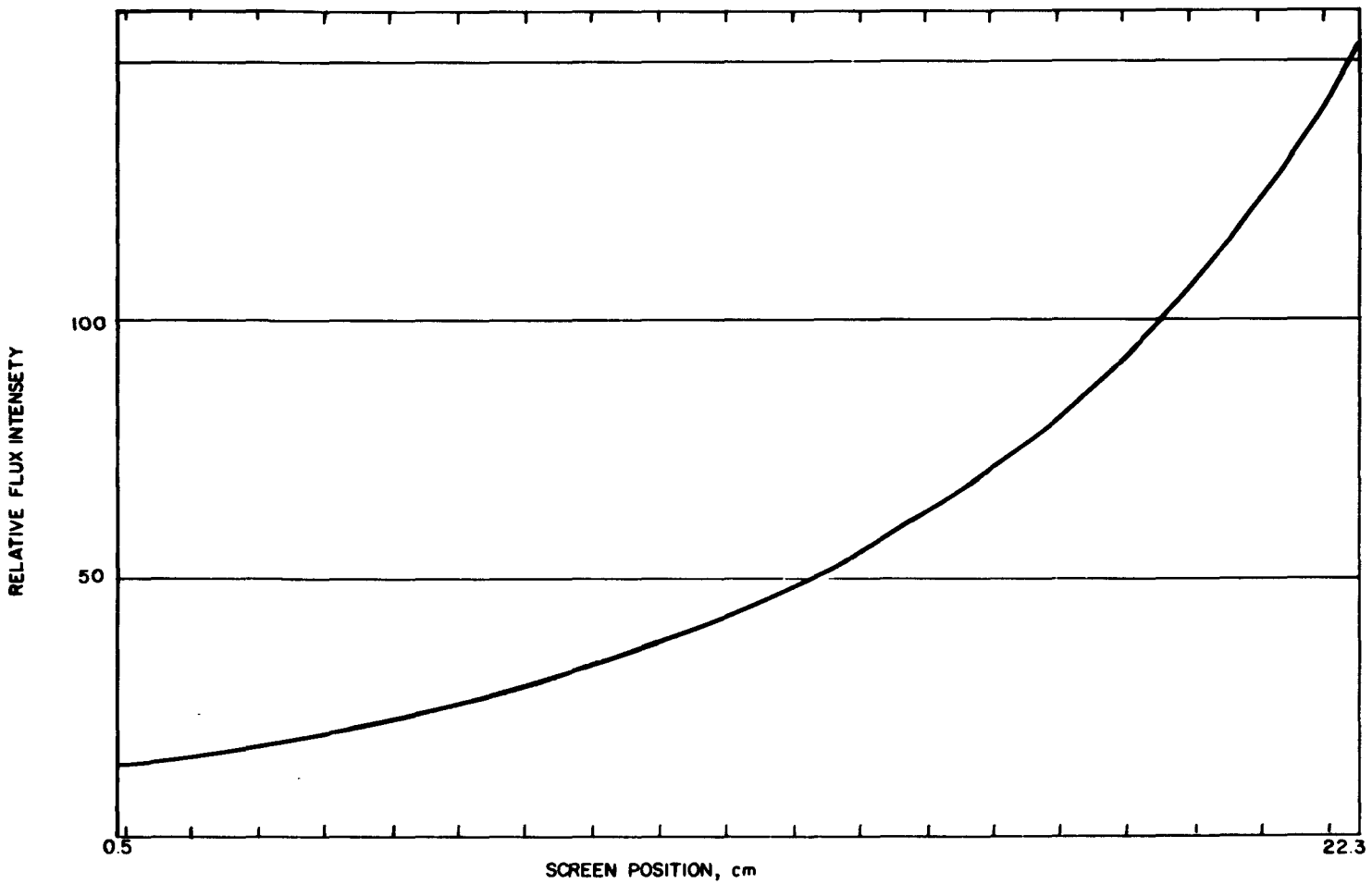

Figure 25 CHANGE OF FLUX VERSUS SCREEN POSITION
63-2167

TABLE VI

LINEARITY OF RADIOMETER SENSITIVITY

MgO Radiometer Coating* No.	Ratios of Radiometer Output				Normal Incidence
	A/B	A/C	A/D	A/E	Ly/min
1	0.64	0.40	0.28	0.22	1.35
2	0.63	0.40	0.28	0.22	1.23
2	0.63	0.39	0.28	0.22	1.35
2	0.64	0.40	0.27	0.22	1.36
3	0.64	0.40	0.28	0.22	1.27
3	0.64	0.41	0.28	0.22	1.27
4	0.63	0.39	0.27	0.21	1.19
4	0.64	0.40	0.27	0.21	1.20
5	0.63	0.40	0.27	0.22	1.03
5	0.64	0.40	0.27	---	1.04
6	0.62	0.39	0.27	0.21	1.06
6	0.63	0.40	0.27	0.22	1.05
7	0.63	0.39	0.26	0.21	0.99
7	0.64	0.37	0.27	0.21	0.97
7	0.63	0.39	0.27	0.22	1.08
7	0.64	0.40	0.27	0.22	1.09
8	0.64	0.39	0.28	0.21	1.07
8	0.63	0.40	0.27	0.22	1.08
9	0.66	0.41	0.29	0.22	0.99
9	0.65	0.41	0.27	0.22	0.97
10	0.64	0.38	0.25	0.21	0.91
10	0.62	0.39	0.25	0.21	0.87
10	0.62	0.37	0.26	0.21	1.12
10	0.63	0.39	0.26	0.22	1.10
AVG.	0.635	0.395	0.270	0.216	---

A = Radiometer output at Flux Attenuator Position 0.5 cm
B = " " " " " " 6.5 cm
C = " " " " " " 12.8 cm
D = " " " " " " 18.1 cm
E = " " " " " " 22.4 cm

* Coating thickness not controlled

The results of a large number of measurements on 50 different MgO coatings proved that it is not possible to focus the microscope sharply on the smooth MgO surface and, accordingly, the precision of the measurement is unsatisfactory. This method of calibration, therefore, was not adapted.

Another approach, however, reducing the sensitivity determination to a single measurement proved to be successful. The method is based on the consideration that the shape of the flux distribution emf record is independent of the coating thickness and of the sensitivity of the radiometer; further, that the peak value of the distribution curve is determined only by the normal solar incidence value and the sensitivity of the radiometer. If the peak values obtained for several coatings of various thickness reduced to unit normal solar incidence coincide, the sensitivity of the instrument is independent of the coating thickness, and it can be obtained by the measurement of the peak value only.

Such sensitivity measurements were performed on 12 different coatings. The results are presented in figure 26, where the peak flux values at the center of the image, as determined by this method, are plotted against the normal solar incidence. The points appear to define well the linear correlation between the two parameters. This proves the assumption that the peak flux readings are dependent solely on the normal solar incidence. This in turn proves that the sensitivity of the instrument is constant throughout the range investigated thus far. Further, it proves that the sensitivity of the instrument is independent of the thickness of the coating. A restriction on the latter statement comes from the statistical analysis of the several hundred coating thickness/sensitivity measurements. It appears that the coating thickness should be kept below 55 microns for the correlation to be valid. It is suggested, therefore, to engrave a mark approximately 55 microns above the sensing disc to insure that coating of suitable thickness is applied.

From figure 26, the sensitivity of the instrument is read as 0.0090 mv/cal/cm^2-sec. A sensitivity of 0.037 mv/cal/cm^2-sec is given by the manufacturer for the camphor soot-coated instrument. The difference between the two values indicates that the camphor black-coated radiometer absorbs four times more radiant energy than the MgO coated one. This finding agrees well with theoretically expected values.

The maximum flux measured with the radiometer was 892 cal/cm^2-sec at 1.38 Ly/min normal incidence. From figure 26, a maximum flux of 975 cal/cm^2-sec is obtained for 1.5 Ly/min normal incidence, the high value for the Boston area. The highest peak flux values in solar furnaces reported thus far are summarized in table VII.

It is realized that the peak flux determined during this work, 975 cal/cm^2-sec, is unexpectedly high, and its validity can be accepted only if proven by a method independent of the described measurement. Such a method was found in checking the melting point of several high refractory compounds in the solar furnace.

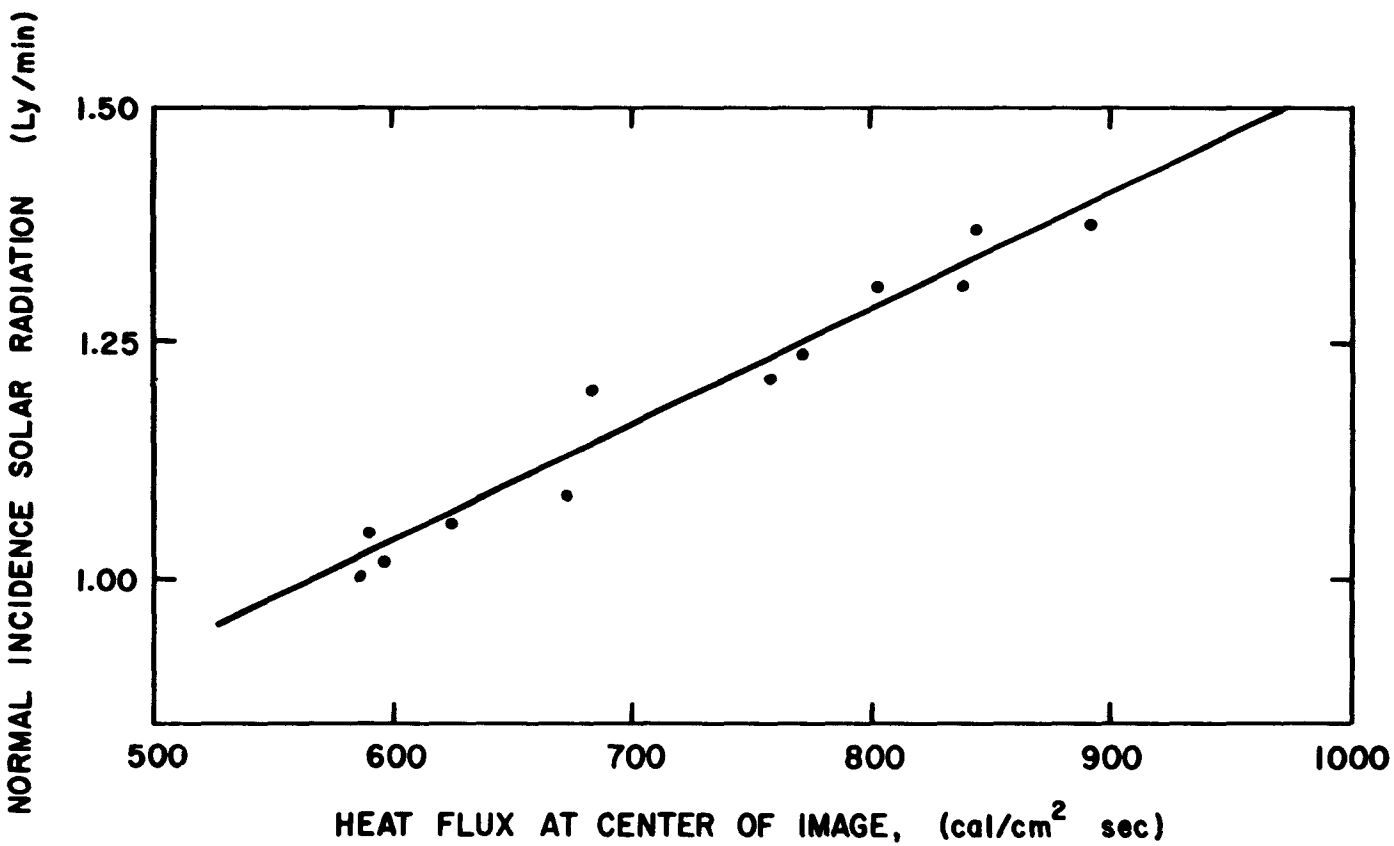

Figure 1 PEAK FLUX VS. NORMAL INCIDENCE SOLAR RADIATION
62-7722

Figure 26 PEAK FLUX VERSUS NORMAL INCIDENCE SOLAR RADIATION
62-7722

If the data presented in figure 26 are true, it should be possible to melt a high refractory compound, e.g., thoria (m.p. 3050° C) at a flux lower than the peak flux obtainable at 1.28 Ly/min normal incidence.

The correlation between flux attenuator position and modulation of peak flux, as shown in figure 25, has been previously determined independently of calorimetic measurements and of the use of a calibrated radiometer. Accordingly, if the peak flux at a given normal incidence is obtained from figure 26, it is possible to reduce it to a desired value by adjusting the flux attenuator. Conversely, if the flux at a given attenuator position is determined by an absolute method, e.g., by the melting of thoria, the peak flux can be arrived at from the known relationship of attenuator position and flux modulation.

TABLE VII

PEAK FLUX IN SOLAR FURNACES

Peak Flux cal/cm^2-sec at 1.5 Ly/min	Method of Determination	Type of Furnace	Reference
573	Measurement	60 inch paraboloid	(13)
638	Calculated from measured average	60 inch paraboloid	(10)
665	Theoretical calculation	105 feet paraboloid mosaic composed of 2 ft x ? [illegible] rical mirrors	(17)
975	Measurement	60 inch paraboloid	present work

Three refractory compounds were selected for use in the checking procedure; alumina, stabilized zirconia, and thoria.

First, the alumina was melted in the solar furnace with a normal incidence of 1.17 Ly/min. It was not possible to freeze the molten alumina under these conditions even when the flux was reduced to the minimum possible value with the flux attenuator. From figure 26, the peak flux at 1.17 Ly/min is 705 cal/cm^2-sec. The attenuator position reduces this value to 148 cal/cm^2-sec.

Assuming an effective emissivity of 0.5, the calculated temperature of the alumina is 2450° C. The fact that the alumina was liquid during this test proves that the temperature was definitely above 2020° C and, thus, the peak flux was higher than 341 cal/cm^2-sec.

The stabilized zirconia was melted with a normal incidence of 1.22 Ly/min with the attenuator in the maximum flux reduction position. From figure 26 the peak flux at 1.22 Ly/min is 746 cal/cm^2-sec. The attenuator position reduces this to 157 cal/cm^2-sec. Assuming an effective emissivity of 0.5, the calculated temperature of the molten sample is 2500° C. According to the supplier of the stabilized zirconia, the melting point is approximately 2590° C. Thus, the peak flux had to be at least 746 cal/cm^2-sec in order to melt the zirconia at the given attenuator position.

The thoria was melted with a normal incidence of 1.28 Ly/min with the attenuator at 9.6 on the arbitrary, linear flux-control scale. The peak flux at 1.28 Ly/min normal incidence is 794 cal/cm^2-sec. The attenuator at the given position reduces this to 293 cal/cm^2-sec. Assuming an effective emissivity of 0.5, the calculated temperature of the molten thoria is 2970° C. This agrees well with the literature data of 3050° C. Thus, the peak flux had to be at least 794 cal/cm^2 sec in order to melt thoria under the experimental conditions.

In these calculations the emissivity value of 0.5 was assumed for the various samples because no reliable information is available. This was taken as a realistic value considering the few data reported in the literature. A difference of ± 0.1 in emissivity does not alter the conclusions drawn from these tests.

As a result of the flux measurement program, it can be stated that under favorable normal solar-incidence conditions in the Boston area (1.00 - 1.40 Ly/min) peak fluxes are available in the 60-inch solar furnace corresponding to a blackbody temperature of 4200° - 4800° C. Under optimum normal solar-incidence conditions (1.40 - 1.50 Ly/min), the available flux corresponds to a blackbody temperature of 4800° - 4900° C. Since the compounds with the known highest melting points are carbides with high emissivities and reported melting points below 4000° C, it appears that it is possible to melt every known solid in the solar furnace.

XII. HEATING OF REFRACTORY OXIDES IN THE SOLAR FURNACE

Several refractory oxides were heated in the 60-inch solar furnace, using a sample holder which permits rotation perpendicular to the optical axis.

Figure 27 shows part of a molten crater of an alumina sample (mp 2050°C). The molten portion is well defined and has a sharp rim produced by quenching the sample. Incipient radial crystal growth is visible at the rim. Specks of impurities are concentrated on the unmelted portion of the alumina. Figure 28 is a cross section through the paraboloidal crater formed by fast spinning of the molten alumina. The voids below the surface were formed during the cooling, crystallization process. Figure 29 shows the cube-like single crystals grown in the voids below the surface. Figure 30 is the photomicrograph of another alumina crater which was heated for a longer period of time and cooled off slowly by moving the flux-control cylinder in small steps. This explains the concentric rings. The hole in the center completes the phonograph record-like appearance. The large voids were formed during the shrinkage and crystallization of the liquid alumina. Figure 31 shows the crater of a zirconia sample (mp 2700° C). The fused surface shows concentric rings caused by decreasing the image size step by step. In figure 32, the sharp definition of the hot zone is demonstrated. The fused crater is surrounded by the original, unmelted porous structure. Figure 33 is a cross section of a zirconia crater. At the surface, a thin, well-defined layer formed during the fast quenching is visible. Underneath, the cooling was slower; and, as a result, somewhat larger and well-defined crystals developed. Figure 34 is a full view of the alumina sample shown partially in figure 27. The impurities diffused away from the hot zone and deposited in a circle at the cooler portion of the sample. The color of the unmelted portion adjoining the crater is much lighter than the original sample, indicating a zone-refining effect.

The same zone-refining effect has been observed when a five-inch long mullite rod was moved back and forth in the image area. After several passages, the center of the rod became much lighter in color, whereas towards both ends dark rings developed, showing an increased concentration of impurities.

Using a stationary sampleholder, thin rods (1/16 and 1/8 inch in diameter) of alumina, zirconia, and thoria were heated in the solar furnace. The rods were exposed head-on to the concentrated radiation, positioned in such fashion that only the center of the rod reached melting temperature. During the heating and consequent cooling, the specimens were observed through a telescope and optical pyrometer alternately through a center hole in the mirror. The radiant flux incident on the samples was changed by small increments with the aid of the control screen. With this technique, it was possible to create at the center of the rod a minute molten pool in contact with the unmolten material.

23x

Figure 27 EDGE OF ALUMINA CRATER

Figure 28 CROSS SECTION OF ALUMINA CRATER 14x

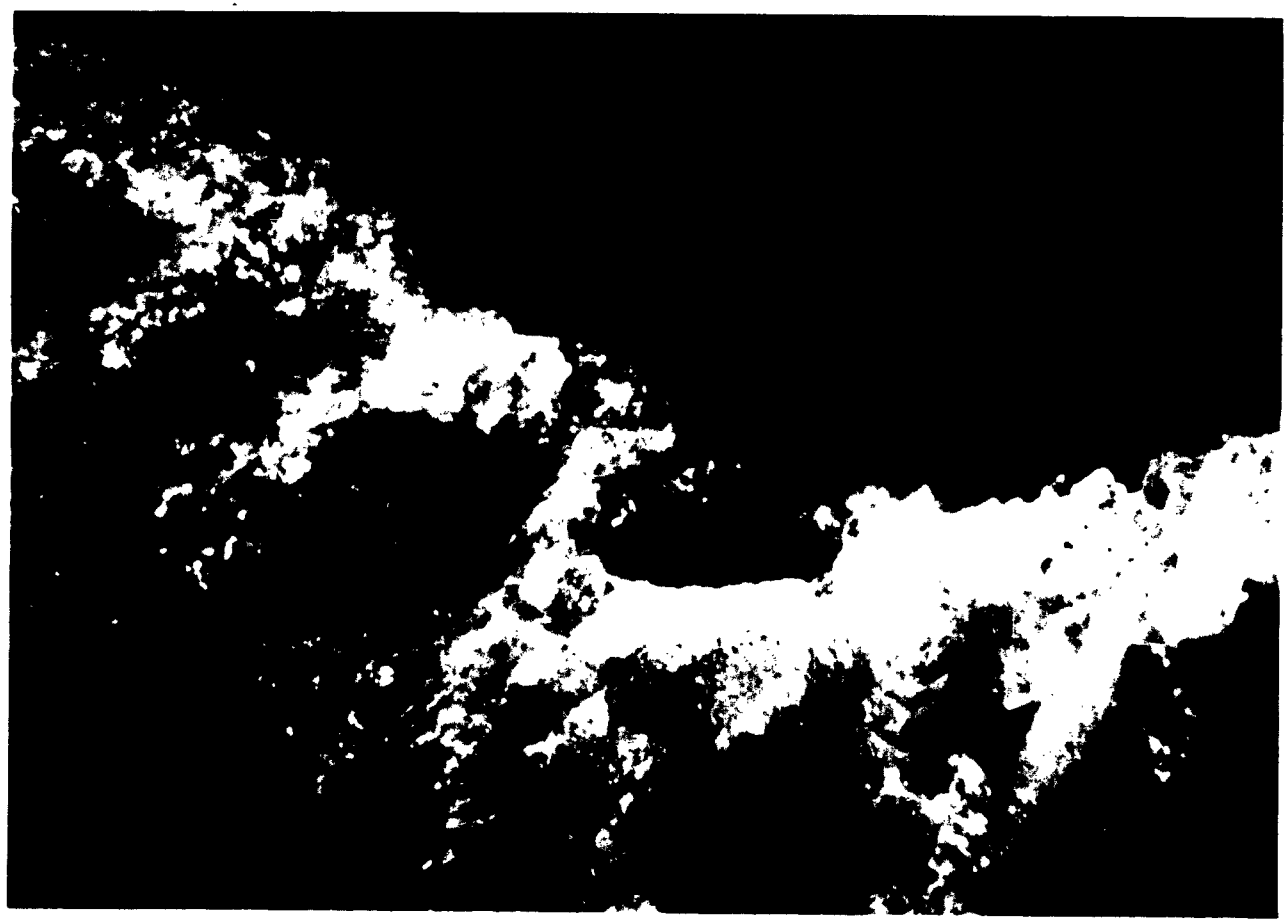

Figure 29 SINGLE CRYSTALS GROWN BELOW CRATER 58x

37x

Figure 30 SLOWLY COOLED ALUMINA CRATER

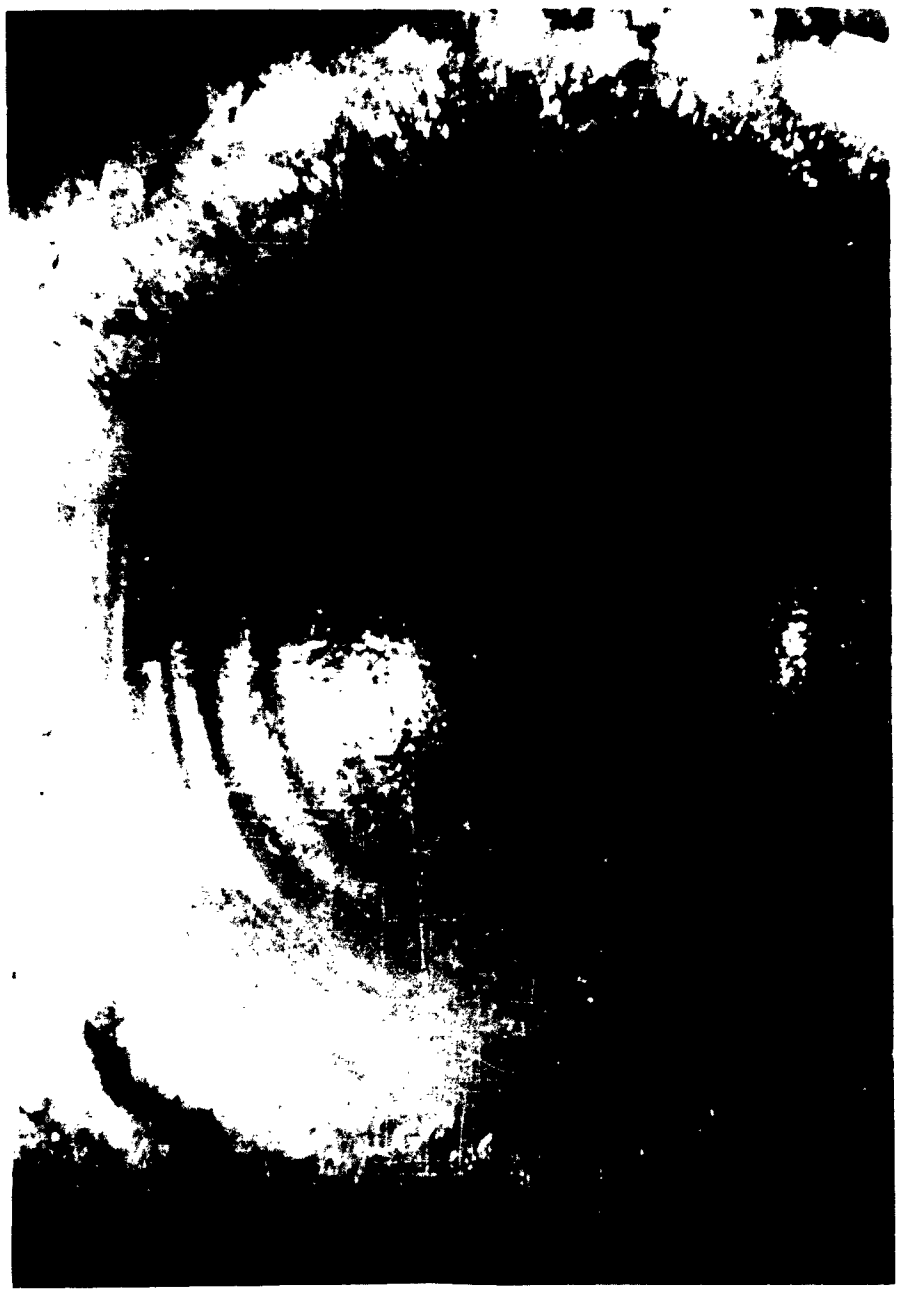

14x

Figure 31 ZIRCONIA CRATER

37x

Figure 32 EDGE OF ZIRCONIA CRATER

58x

Figure 33 ZIRCONIA CRYSTALS GROWN BELOW CRATER

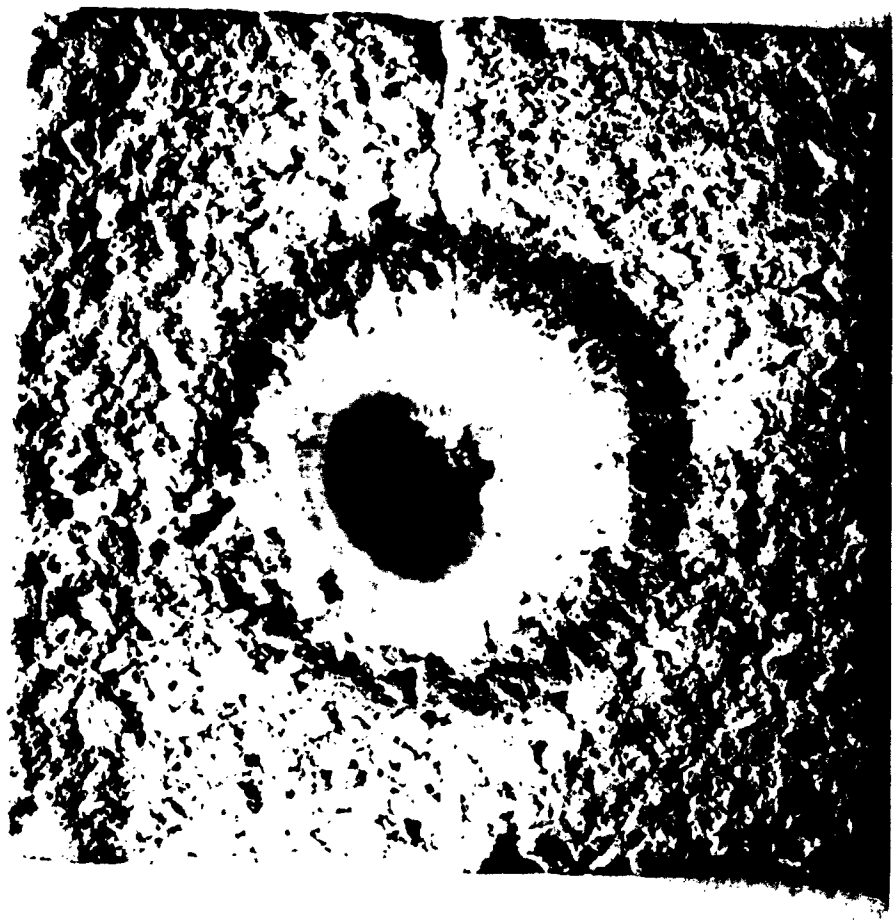

2 1/2x

Figure 34 ZONE EFFECT ON ALUMINA CRATER
P-6093

When the thoria rods were exposed to fluxes much greater than those necessary for melting, the thoria vaporized at a very rapid rate. The vapors condensed upon reaching the cooler portion of the sample at the edge of the focal area. As a result of the condensation, single crystals and crystal clusters were formed at the periphery of the crater (figure 35). Figure 36 shows a rod-like single crystal with sharply defined faces on the top. Figure 37 is an octohedral single crystal attached to the sample by a thread-like formation. Figure 38 presents several crystal clusters composed of similar sizes. Figure 39 shows also twining along the c axis, but the crystals are ordered in decreasing size. Figure 40 is a photograph of small crystals in dendritic growth but well defined crystal habit.

Figure 35 CONDENSATION CRYSTALS AROUND THORIA CRATER 16x

160x

Figure 36 ROD-LIKE SINGLE CRYSTALS OF THORIA

255x

Figure 37 OCTOHEDRAL SINGLE CRYSTAL OF THORIA

160x

Figure 38 THORIA CRYSTAL CLUSTER

Figure 39 MULTIPLE TWIN THORIA CRYSTALS 160x

255x

Figure 40 DENDRITIC THORIA CRYSTALS

XIII. THE MEASUREMENT OF THE ELECTRICAL RESISTIVITY OF REFRACTORY OXIDES

Electrical resistivity measurements of refractory oxides at high temperatures present a number of problems which are difficult to solve. The heating of such materials is usually accomplished by radiation from a resistively or inductively heated conductor. At high temperatures, the conductor has to be heated in vacuum or inert atmosphere. It has been observed, however, [18] that the conductivity of alumina increased with time when heated in vacuum at a constant high temperature. The explanation offered by Hartmann was that alumina dissociates when heated in vacuum thus causing an increase in conductivity. When it is reheated in air, the conductivity decreases to the original value. A further drawback of such heating is the volatility of the heating elements and other parts of the furnace. Whether the heating takes place in vacuo or inert atmosphere, the vapors of the heater may introduce impurities into the sample.

In high temperature furnaces, thermionic emission occurs at the surface of all heated parts. This emission may produce a shunt effect which can render the resultant resistivity values meaningless. [19] Operating in vacuo naturally tends to increase emission.

The electrical contacts required for resistivity measurements also cause difficulties. Since the metallic contacts are at the same high temperature as the sample, reaction between the two is both possible and probable. Cooled metallic contacts, on the other hand, cannot be used as the resultant heat loss would upset the temperature uniformity of the sample.

If the conductor is heated by induction, the high-frequency electromagnetic field may also interfere with the measurements.

It appears that the measurement of electrical resistivity of oxides at high temperature in an image furnace does not raise these difficulties. A sample can be heated in any atmosphere, including air. The concentrated radiant energy heats only the sample and no other part of the furnace. As a result, no contaminating reaction can take place and thermal emission is restricted to the sample surface.

The metallic contacts are not heated and thus no reaction at the interface can occur. If required, the metal contacts can be liquid cooled; and the resulting effect on the temperature distribution is considered together with the uneven temperature distribution specific to image furnaces. There is also no electromagnetic field surrounding the sample which would interfere with measurements.

An experimental program was carried out in order to prove the suitability of image furnaces for the measurement of the electrical resistivity of oxides. Alumina was chosen for this program because it can be easily obtained in high purity; it can be formed into any shape by conventional techniques, and its electrical resistivity has been measured up to 1500° C by several investigators.[19] Samples were prepared from 99.5 percent pure Al_2O_3 by ball milling and by both slip casting and hydraulic pressing, using an organic binder. The shapes were prefired at 1100° C and machined to the desired dimensions. The final firing was made in an induction furnace at 1750° C, using a tungsten susceptor with an alumina lining. The samples were of cylindrical shape, with two slots at the bases to engage with the drive key of the sample holder jaws. The following sample sizes were fabricated:

Length	Diameter
1.000 inch	0.875 inch
1.000 inch	0.625 inch
0.750 inch	0.500 inch
0.500 inch	0.375 inch
0.450 inch	0.335 inch

These samples were mounted in the sample holder (shown in figure 5) and exposed to the concentrated solar radiation. It was observed that with the four longest samples a portion of the sample was outside the focal area. The 0.450-inch long sample was found to be suitable in length and diameter to obtain the desired temperature distribution lengthwise as well as the maximum heated area about its circumference.

This size of sample was used for all successive heating and measuring tests in the solar furnace. During the heating, the sample was rotated perpendicular to the optical axis of the solar furnace in order to obtain maximum temperature uniformity across its diameter. The brightness temperature was observed with a PYRO micro-optical pyrometer. The pyrometer was mounted on a micrometer slideway in such a fashion that it could be displaced perpendicularly to the optical axis of the furnace by measured small increments. Thus the temperature distribution along the sample could be measured with a fine resolution. The sample-holder jaws were not affected by the proximity of the hot zone, and the cooling transformer oil did not heat up perceptibly.

The radiation observed with the optical pyrometer included both the radiation emitted by the hot sample and the solar radiation reflected by the sample. Thus the temperature readings could not be interpreted as the temperature of the sample. In order to make meaningful temperature measurements, a rotating sector based on a design of Conn and Braught[20] was used to separate the emitted radiation from the reflected solar radiation. A sketch of the rotating sector is shown in figure 41. In operation, the sector is rotated at a speed of 200 c/sec by a synchronous motor through a nonslip drive belt. When the specimen, the

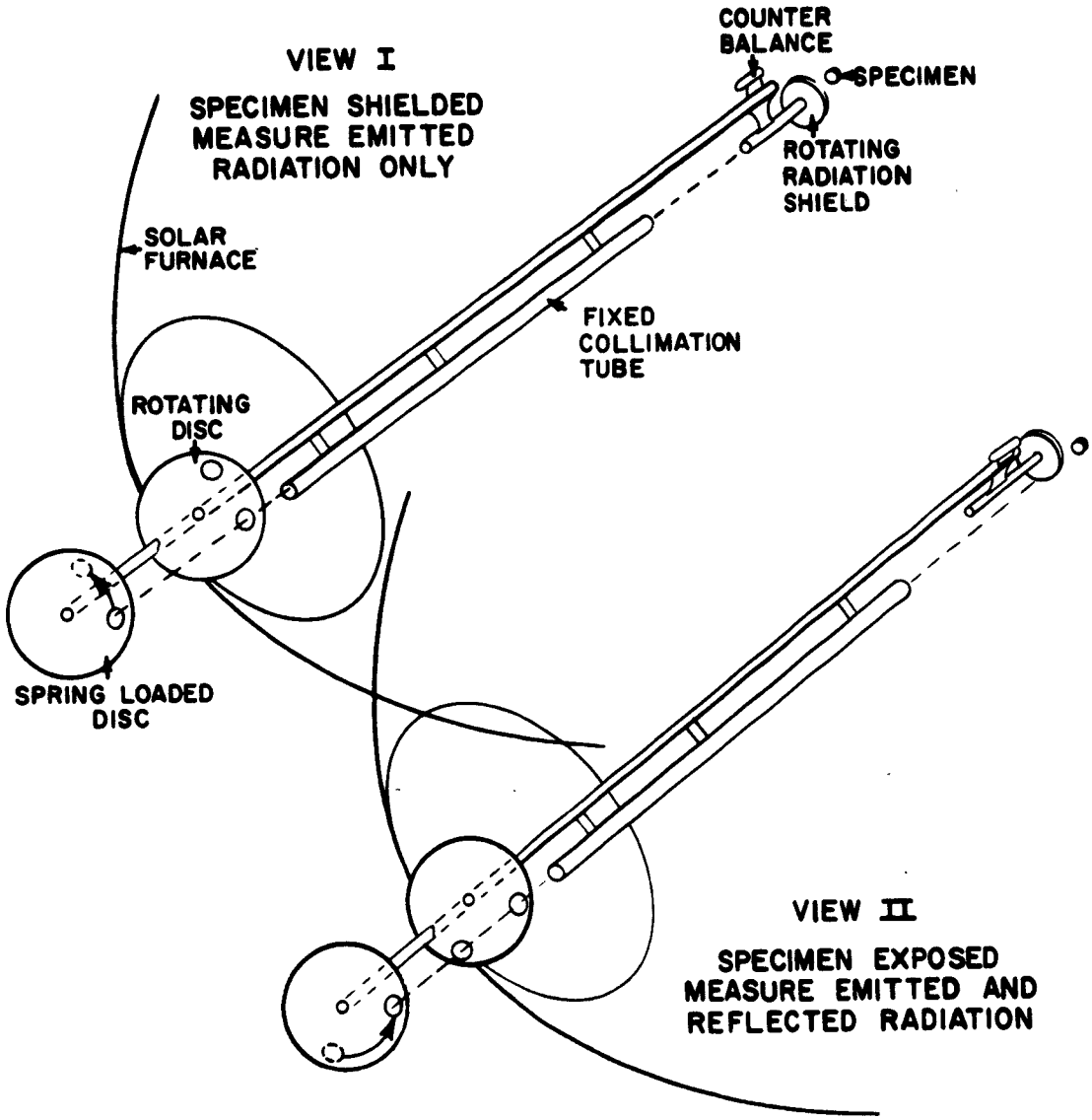

Figure 41 OPERATION OF ROTATING SECTOR
62-8929

rotating shield, and the orifices of both discs all are aligned, no solar radiation falls on the specimen, and only the radiation emitted by it reaches the radiation detector. When the spring-loaded disc is retarded, however, it transmits radiation from the specimen while it is heated by solar radiation. Thus, the emitted plus-reflected radiation reaches the detector.

The sample was heated in the solar furnace with the rotating sector in operation. The temperature distribution along the sample was measured with the optical pyrometer. The results of such a measurement are presented in figure 42. This temperature distribution was observed with the flux-control screen at the minimum-flux position. By repositioning the control screen, the maximum temperature can be increased in discrete steps while the temperature at the ends is held constant by the cooled contacts. Thus, the conditions for the calculation of the temperature dependence of the measured property described in section IX are fulfilled.

The resistance of the heated samples was measured with an Industrial Instruments Model L-7 megohmmeter and a standard vacuum-tube voltmeter. The resistance of a 0.450-inch long, 0.335-inch diameter alumina sample having a brightness temperature distribution shown in figure 42 was measured using applied voltages of 2-1/2, 150, 250, and 350 volts. The following values were obtained:

Test voltage	Resistance
2-1/2	2.00×10^8 ohm
150	1.80×10^8 ohm
250	1.75×10^8 ohm
350	1.80×10^8 ohm

The polarity was reversed several times during these measurements. With the high-test voltages, no change in resistance was observed with the reversal of polarity. With the 2-1/2-volt tests, however, the polarity reversal increased the resistivity to 4.50×10^8 ohms. The resistance increase was not permanent, and a decrease with time was observed. A similar observation was reported by Arizumi and Tani,[21] who attributed this to the presence of ionic currents in the alumina.

In figure 42, brightness temperatures are shown as measured directly on the optical pyrometer. Emittance values for the alumina sample are necessary to convert these to true temperatures. No emittance values are available in the literature which would be applicable to a particular sample of given composition, crystal structure, and surface conditions. Separate investigations in this laboratory are in progress in order to establish a method for the measurement of emittance at high temperatures. It appears possible to perform the emittance measurements simultaneously with the measurement of other high temperature properties. Thus, such emittance values will be obtained which are directly applicable to the calculation of the true temperature of the sample at which the high temperature property was measured.

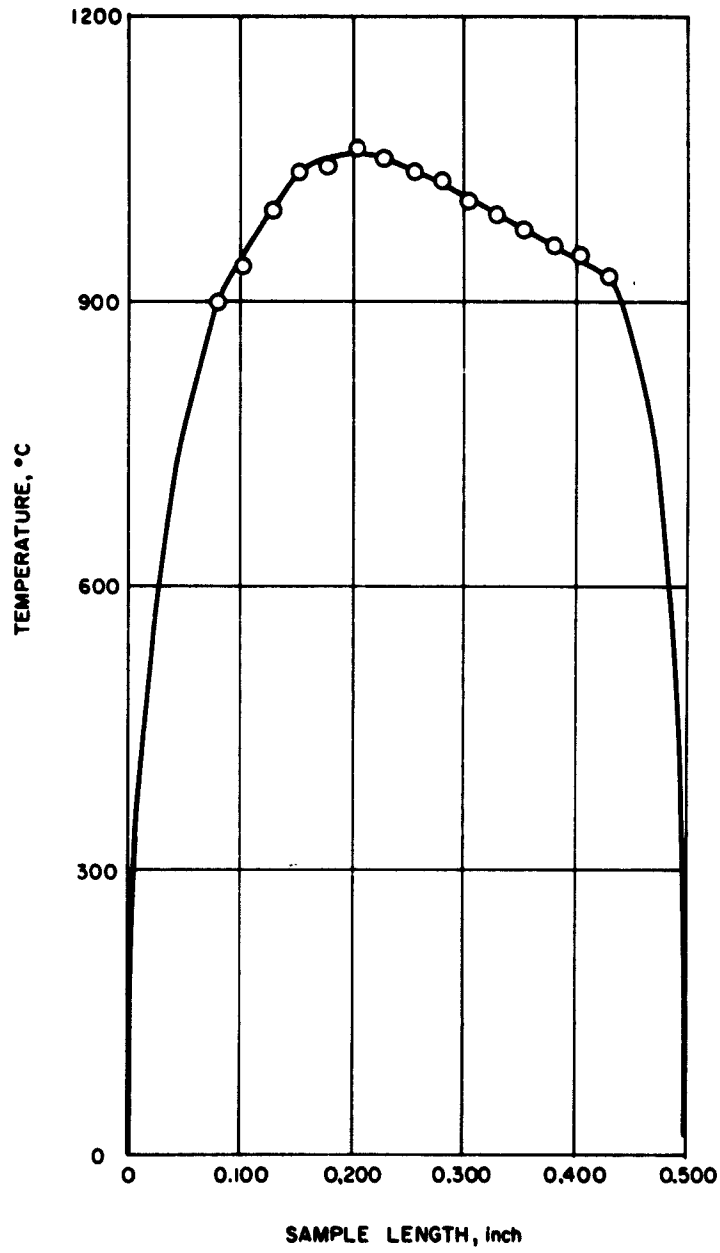

Figure 42 UNCORRECTED OPTICAL PYROMETER READINGS ALONG SAMPLE 63-2340

After the true temperature distribution of the sample is known, the flux is changed in order to alter the peak temperature. With this new flux setting, another resistance and temperature distribution measurement is made. The same procedure is repeated as many times with as small peak temperature changes as required for the application of the method outlined in section IX. Thus, the temperature dependence of the electrical resistivity of the sample can be determined.

XIV. DELIVERIES

In accordance with the requirements of the contract, the following items were delivered to the contracting agency:

1. Prototype model of vacuum and gas-filled image chamber
2. Thirty-six-inch diameter paraboloidal reflector
3. Engineering drawings:

   LA-2923, Solar Furnace Shutter-Design Study No. 2

   LA-2924, Sensing Element-Guiding Mechanism

   LA-2925, Shutter-Solar Furnace

   LA-2926, Furnace-Solar

   LA-2927, Solar Furnace-Guiding System

   LA-2700, Sample Holder-Solar Furnace

XV. VISITS

Visits were made by the principal investigator to several laboratories where similar research activity is in progress. The following organizations were visited:

Naval Radiation Defense Laboratory, San Francisco, California.
Stanford Research Institute, Menlo Park, California.
Holloman Air Force Base, New Mexico.
Material Laboratory, Naval Shipyard, Brooklyn, New York.
Arthur D. Little, Inc., Cambridge, Mass.
Laboratoire de L'Energie Solaire, Montlouis, France.

The problems of image furnace techniques were discussed at great length with the scientific personnel of these organizations. Their interest and cooperation is greatly appreciated.

XVI. PUBLICATIONS

The following is a list of publications where partial or total sponsorship of this contract has been acknowledged:

Anonym., New England Supplies Fuel for Solar Furnace New England Professional Engineer 13 (5), 4-6 (1960).

Laszlo, T. S., High Temperature Physics and Chemistry Lecture series, The American University, Washington, D. C. (29 June - 1 July 1960).

Laszlo, T. S. and M. S. Klamkin, Determination of the Temperature Dependence of Material Properties in Image Furnaces, AFCRL-TN-60-797, (18 October 1950); Solar Energy 4 (3), 20-21 (1960).

Laszlo, T. S., On Radiant Energy in High Temperature Research, presented at the annual meeting of the American Society of Mechanical Engineer New York City, (30 November 1960); Solar Energy, Vol V, No. 4 (October - December 1961).

Laszlo, T. S. Image Furnaces for High Temperature Research, presented at the meeting of the Boston Section of The Electrochemical Society (23 February 1961).

Laszlo, T. S., Present Status and Prospects of High Temperature Research with the Solar Furnace, Solar Energy Symposium, University of Florida, Gainesville, Florida, (11 April, 1961).

Laszlo, T. S., and P. J. Sheehan Jr., Final Report-Investigation of Thermal Imaging Techniques AFCRL 131, (18 April 1961).

Laszlo, T. S. High Temperature Physics and Chemistry Lecture Series, The American University, Washington, D. C. (28-30 June 1961).

Laszlo, T. S., Measurement and Application of High Heat Fluxes in a Solar Furnace, presented at the XVIII International Congress of Pure and Applied Chemistry, Montreal, Canada; (9 August 1961), Solar Energy, Vol. VI No. 2, 69 (1962).

Laszlo, T. S., and M. S. Klamkin, Analytical Evaluation of a New Shape Artifical Blackbody (tentative title-to be published).

Laszlo, T. S. New Techniques and Possibilities in Solar Furnaces, presented at the United Nations Conference on New Sources of Energy, Rome, Italy (21-31 August 1961).

PUBLICATIONS (Concl'd)

Laszlo, T. S., Solar Energy in High Temperature Research, presented at the NATO Advanced Study Institute for Solar and Aeolian Energy, Sounion, Greece. (4-17 September 1961).

Laszlo, T. S., Utilization of Solar Energy, presented at the Science Congress organized by the Department of Education of the Commonwealth of Massachusetts and the IAE, (2 June 1962).

Laszlo, T. S., High Temperature Physics and Chemistry Lecture Series, The American University, (27-29 June 1962).

Laszlo, T. S., and P. J. Sheehan, Investigations of Thermal Imaging Techniques, presented at " A Conference of Imaging Techniques" Cambridge, Massachusetts. (4-5 October, 1962).

Laszlo, T. S., P. J. Sheehan, Sample Holder for Electrical Measurements, technical note to be published in Solar Energy.

Laszlo, T. S., P. J. Sheehan, Radiometer Calibration, technical note to be published in Solar Energy.

Laszlo, T.S., Image Furnace Techniques, to be published in the series Techniques of Inorganic Chemistry, edited by Jonassen and Weissberger, published by John Wiley and Sons, Inc.

XVII. REFERENCES

1. Laszlo, T. S., Solar Furnace in High-Temperature Research, Science 124, 797 (1956).

2. Laszlo, T. S., and P. J. Sheehan, Final Report-Investigation of Thermal Imaging Techniques, RAD-TR-61-9, AFCRL 131, (18 April 1961).

3. Glaser, P. E., Engineering Research with a Solar Furnace, J. Solar Energy 2, 7 (1958).

4. Davies, J. M., and E. S. Cotton, Design of the Quartermaster Solar Furnace, J. Solar Energy 1, 16 (1957).

5. Gubareff, G. G., J. E. Janssen, and R. H. Torborg, Thermal Radiation Properties Survey, Honeywell Research Center, Minneapolis, Minn. (1960).

6a. Gillette, R., H. E. Snyder, and T. Timar, Lightweight Solar Concentrator Development, Solar Energy V, No. 1, 24 (1961).

6b. Bolin, J., C. J. Tenukest, and C. J. Milner, Plastic-Replica Mirror Segments for a Solar Furnace, Solar Energy V, No. 3, 99 (1961).

6c. Bradford, A. P., W. W. Erbe, and G. Hass, Two-Step Method for Producing Replica Mirrors with Epoxy Resins, J. Opt. Soc. Am. 49, No. 10, 990 (1959).

6d. Saxton, J. H., and D. E. Kline, Optical Characteristics and Physical Properties of Filled-Epoxy Mirrors, J. Opt. Soc. Am. 50, 1103 (1960).

7. Archibald, P. B., A Method for Manufacturing Parabolic Mirrors, J. Solar Energy 1, 102 (1957).

8. Khanna, M. L., USSR Solar Energy Exhibit, The Sun at Work VII, No. 1, 4, (1962).

9. Glaser, P. E., M. M. Chen, and J. Berkowitz-Mattuck, The Flux Redistributor, Solar Energy VII, No. 1, 12 (1963).

10. Farber, J., Images of Very High Temperature Sources, Symposium on High Temperature-A Tool for the Future, Stanford Research Institute, (1956).

11. Buckley, H., On the Radiation from the Inside of a Circular Cylinder, Phil. Magazine, 4, 753 (1927); 6, 447 (1928); 17, 576 (1934).

REFERENCES (Concl'd)

12. Gouffé, A., Corrections d'ouverture des corps-noir artificiels compte tenu des difussions multiples internes, Revue D'Optique, 24 (1-3), 1 (January - March 1945).

13. Jacquez. J. A., and H. F. Kuppenheim, Theory of the Integrating Sphere, J. O. Soc. Am. 45, No. 6, 460 (1955).

14. Laszlo, T. S., Temperature and Flux versus Geometrical Perfection, Solar Energy, 1, 78 (April - July 1957).

15. Knowles Middleton, W. E., and C. L. Sanders, The Absolute Spectral Diffuse Reflectance of Magnesium Oxide, J. Opt. Soc. Am., Vol. 41, No. 6, (1951) p. 149.

16. Gardon, R., An Instrument for the Direct Measurement of Intense Thermal Radiation, Rev. Sci. Inst., 24, 266, (1953).

17. Allison, F., H. Carr, and G. Hughes, Notes on the Potential Performance of the Cloudcroft Solar Furnace, Solar Furnace Support Studies, AFMDC, TR 58-7, AD 135014 (1958).

18. Hartmann, W., Z. Physik., 102, 709 (1936).

19a. Podszus, E., Zeitchsrift fur Elektrochemie, Vol. 39, p. 75, (1933).

19b. Cohen, J., Electrical Properties of Sapphire, Contract NONR - 1840(00), Sylvania Electric Products Quarterly Report, No. YD 57-6-10, (15 May - 15 August 1958).

19c. Budnikov, et al, Method of Measuring Electric Conductivity of Ceramic Materials at High Temperatures, Ogneupory, Nos. 5-6, (May - June 1962).

19d. Heldt, K., and G. Haase, Der Elektrische Widerstand von Reinem Hochvakuumgesintertem Aluminiumoxyd, Z. Angew. Phys. 6, 157, (1954).

20. Conn. W., and G. Braught, Separation of Incident and Emitted Radiations in a Solar Furnace By Means of Rotating Sectors, J. Opt. Soc., Vol. 47, No. 1, 45, (January 1954).

21. Arizumi, T., and S. Tani, J. Phys. Soc., Japan, 6, 55, (1951).

APPENDIX

IMAGE FURNACE TECHNIQUES SURVEY

Image furnaces have found wide application recently in high temperature research and testing. Because of their peculiar characteristics, new instruments, experimental set-ups, and methods had to be found for their successful operation. Some of this recently developed knowledge has been published in different journals, proceedings, and research reports, but most of the results are not widely available. As a consequence, investigators have to devote much time and effort to solve those instrumentation and procedural problems which have already been solved by others. Worse still, the distinct advantages of using image furnace techniques for the solution of some very difficult experimental problems are not even recognized in many cases.

A survey work was therefore initiated with the intention of remedying this situation. In addition to a thorough literature search, all organizations known to be active in this field were requested to supply information about recent investigations, including new techniques and instrumentation, special problems encountered, and so forth. Altogether, 129 organizations were contacted, and technical information has been received from 70.

The first result of the survey is presented in a tabulated form listing the location of the facility together with a few pertinent data.

The technical material is presently undergoing a systematic arrangement, beginning with the discussion of various radiation sources and ending with the description of experiments performed in image furnaces. The information will be presented in such manner that a newcomer to the field should be able to decide whether imaging techniques are suitable to his research problem. In the case of a positive answer, he should be able to select the equipment and methods best suited to his needs. For the experienced investigator, in turn, there will be enough details included on specific experimental setups and methods to aid in solving his particular problems and to compare his approach to that of others.

The entire survey will be published under the title, "Image Furnace Techniques", in the series Technique of Inorganic Chemistry, edited by Jonassen and Weissberger, to be published by John Wiley & Sons, Inc.

IMAGE FURNACE FACILITIES

Name and Address	Investigators	Optical System	Source	Maximum Image Flux	Reactions and Experiments
ALGERIA					
Institute de l'Energie Solaire de l'Universite de'Alger, Algiers	Perrot G. Vuillard M. Touchais J. Francois	8.40-m dia. parabolic concentrator. 1.5-m dia. silvered glass paraboloid 46.6-cm dia. metal mirror	Sun		Photochemical research, thermionic generator. Preparation of boron carbide.
AUSTRALIA					
Chemical Research Laboratories, Melbourne.	J. H. Weymouth	60-in paraboloidal with heliostat	Sun		Investigation of the high lime end of such systems as $CaO-TiO_2$, $CaO-ZrO_2$, $CaO-CeO_2$, $CaO-ThO_2$.
The University of New South Wales, Kensington, N. S. W.	Prof. C. J. Milner J. W. Ciutronich	12-ft dia. parboloidal reflector with heliostat	Sun		Investigations of the physical and mechanical properties of tungsten.
BELGIUM					
Free University of Brussels, Brussels	P. Goldfinger J. Drowart	Double elliptical glass mirrors	Carbon arc		Vaporization studies.
CANADA					
Defence Research Chemical Laboratories, Ottawa	L. G. Wilson G. Drew	Cassegrain type with 60-in back silvered parabolic primary mirror and a 15-in dia. aluminized hyperboloid second mirror	Sun	200 cal/cm^2/sec	Study of materials used to protect men and equipment from the thermal radiation of atomic weapons.
ENGLAND					
Morganite Research & Development Ltd., London	Kennedy G. McWhirter D. R. Lovell R. F. Hilton	Two coaxially mounted 60-in parabolic concentrator	Carbon arc	120 cal/cm^2/sec	Melting of refractory materials.
Pilkington Brothers, Ltd., St. Helens, Lancs.	L. H. A. Pilkington	150-cm dia. pyrex glass reflector	Carbon arc		Fusing of oxides.
Rocket Propulsion Establishment, Ministry of Aviation, Westcott, Buckshire.	J. D. Lewis	Two coaxial paraboidal mirrors	Carbon arc	250 cal/cm^2/sec	Sample ignition studies.
United Kingdom Atomic Energy Authority, Sheffield	P. Murray	16-in double ellipsoidal rear surface silvered mirrors	Carbon arc		Fusing of refractory oxides. Study of fission gas release of irradiated ceramic oxides.
University of Exeter, Exeter	M. B. Small J. R. Drabble	Double ellipsoidal reflectors	Carbon arc		The growth of high-purity single crystals of transition metal oxides.
University of Sheffield, Sheffield	I. A. McGrath T. G. Carruthers	Two 150-cm dia. paraboloid reflectors	Carbon arc	300 cal/cm^2/sec	Preparation of melts for equilibrium diagram studies.
FRANCE					
Laboratoire de L'Energie Solaire, Montlouis,	M. Foex M. Trombe	100-foot parabolic concentrator with heliostat, 6 six-foot parabolic concentrators with heliostats	Sun		Research and semi-industrial applications.
Societe La Carbone - Lorraine Epinay - Sur - Seine, Seine	E. Fourquin	Double elliptical mirrors (14-in dia.)	Carbon arc	Temperatures over 2500°C	Investigations of carbon, graphite.
Sud-Aviation Courbevoie, Seine	C. Thomas	Two 1500-mm dia. parabolic concentrators	Carbon arc		Measurement of thermal diffusivity of ablative materials and thermal resistance of contacts; study of thermal decomposition products.
GERMANY					
University of Freiburg, Freiburg	Prof. B. Brauer	Paraboidal concentrator	Sun		Thermal dissociation of metal oxides (TiO_2), measurement of O_2 equilibrium pressure.
INDIA					
National Physical Laboratory, New Delhi	M. L. Khanna	Paraboidal concentrator	Sun	1.5 cal/cm^2/sec	Concentration of palm and cane juices.
JAPAN					
Central Research Lab., Tokyo Shibaura Electric Co., Ltd. Kawasaki	F. Nagatani	Two 21-in ellipsoidal mirrors.	Carbon arc	325 cal/cm^2/sec	Crystallization of metal nitrides.
Tohoku University, Sendai	T. Sakurai	10-m. dia. paraboidal concentrator with heliostat	Sun		
Government Industrial Research Institute, Nagoya.	T. Noguchi M. Yoshida T. Kozuka	150-cm dia. paraboidal mirror with heliostat	Sun		Vacuum fusion of oxides.
NETHERLANDS					
Phillips Research Laboratories, Eindhoven	C. Kooy	36-in chain glass, elliptical mirrors	Carbon arc	5 w/mm^2 estimated	Zone melting of ferromanganate, TiO_2 and NiO. Growing of single crystals.

IMAGE FURNACE FACILITIES (Cont'd)

Name and Address	Investigators	Optical System	Source	Maximum Image Flux	Reactions and Experiments
U. S. A.					
A. D. Little Inc. Cambridge, Mass.	P. E. Glaser D. F. Comstock D. L. Richardson	21-in dia. ellipsoidal and paraboloidal mirrors, 36-in dia. paraboloidal mirrors	Blown arc, graphite resistor xenon lamp	250 cal/cm^2/sec	Pyrolysis studies; measurements of emissivity, thermal conductivity, etc.
Aeronautical Systems Division, USAF, Wright-Patterson Air Force Base, Ohio.	R. Farmer H. Marcus	Double ellipsoidal, with 21-in mirrors, quartz condenser	Carbon arc	240 cal/cm^2/sec 30 cal/cm^2/sec uniform	Ablative performance of plastics in high irradiance environments. Thermal diffusivity studies. Thermal radiation of mice.
Air Research Manufacturing of Arizona, Phoenix, Arizona	J. W. McDonald	60-in dia. paraboloid	Sun	1000 Btu/ft^2/sec 1/6-in dia. circular area	Evaluation of solar turboelectric power plant.
Air Force Cambridge Research Laboratories, Bedford, Mass.	G. P. Pleets	36-in and 60-in dia. paraboidal concentrators	Carbon arc		Investigations of 3-phase ac carbon arc.
Air Force Office of Scientific Research, Holloman AFB, New Mexico	Dr. P. D. Jose	60-in paraboidal concentrator with heliostat.	Sun		Investigation of experimental techniques.
Army Signal Research and Development Laboratory, Fort Monmouth, N. J.	J. P. Angello A. Herchakowski	21-in ellipsoidal reflectors	Carbon arc	1260 Btu/ft^2/sec	Development of experimental thermionic diodes; investigation of solar cell characteristics at various light intensities.
Atlantic Research Corp., Alexandria, Va.	J. D. Batchelor	Two 60-in parabolic mirrors	Carbon arc	300 Btu/ft^2/sec	Thermal testing of ablative type reinforced plastic insulation.
Avco RAD. Wilmington, Mass.	T. S. Lazzio P. J. Sheehan	60-in paraboidal concentrator	Sun	950 cal/cm^2/sec	Calorimetric and radiometric flux measurements. Measurement of electrical resistivity and emittance. Study of refractory materials.
Bermite Powder Co., Saugus, California	L. LoFiego	Two 16.5-in ellipsoidal mirrors	Carbon arc	125 cal/cm^2/sec	Threshold ignition values and burning rate exponents of propellants; deflagration to detonation transition in primary explosives.
Boeing Company, Seattle, Washington		60-in parabolic mirrors 36-in parabolic mirrors	Carbon arc 10,000 watt tungsten filament lamp	180 Btu/ft^2/sec	
Bureau of Mines, U. S. Albany Metallurgy Research Center, Albany, Oregon	H. J. Kelley	Back silvered pyrex ellipsoidal reflectors	Carbon arc		Growth of single crystals.
Bureau of Mines, U. S. College Park Research Center, College Park, Md.	L. R. Furlong E. R. Maust, Jr.	Two 60-in dia. paraboloid	Graphite resistor or carbon arc	200 cal/cm^2/sec	Melting points of some refractory materials.
Corning Glass Works, Corning, New York	W. H. Dumbaugh Jr.	Two 60-in parabolic mirrors	Carbon arc		Material research at high temperature.
Douglas Aircraft Co. Santa Monica, Calif.	A. C. Rawsha	21-in ellipsoidal reflectors	Carbon arc	325 cal/cm^2/sec	Measurement of thermophysical and thermoradiative properties of refractory metallic and non-metallic materials.
Dow Chemical Company, Midland, Michigan	H. Prophet	21-in dia. elliptical mirrors	Carbon arc	330 cal/cm^2/sec	Heat capacity and enthalpy measurements above 1300°F.
General Electric Co. Missiles and Space Vehicle Dept., Philadelphia, Pa.	H. L. Friedman	Two coaxially mounted 60-in parabolic reflectors	Carbon arc	435 Btu/ft^2/sec	Pyrolysis of plastics
General Telephone and Electronic Laboratories, Inc., Bayside, N. Y.	L. Seigle, R. Resnick H. Stemitz	Double elliptical mirrors	Carbon arc	270 cal/cm^2/sec	Cooling of tungsten structures by evaporation of infiltrated material.
Goodyear Tire and Rubber Company, Akron, Ohio	M. Conger	21-in ellipsoidal mirror	Carbon arc	325 cal/cm^2/sec	Development of improved ablative, elastromeric insulation for rocket motor cases.
Iowa State University, Ames Iowa	D. R. Wilder	21-in ellipsoidal mirrors	Carbon arc	300 cal/cm^2/sec	Study of grain-growth phenomena in uranis filled elements. Measurement of emissivity and heat capacity.
Jet Propulsion Laboratory, California Institute of Technology, Pasadena, California	Howard E. Martens	21-in ellipsoidal mirrors	Carbon arc	300 cal/cm^2/sec	Degradation studies of polymer materials at different flux levels
Lockheed Missiles and Space Company Research Laboratories, Palo Alto, California	W. G. Bradshaw J. Crank R. E. Rolling	36-in paraboloid concentrator	Carbon arc		Measurement of surface recession rates, and char formation in ablative materials. Oxidation and sublimation rate observation.
Martin Company, Baltimore, Md.	J. W. Maccallous E. L. Strauss F. W. Paul	Two 14-in dia. ellipsoidal mirrors	Carbon arc	200 Btu/ft^2/sec	Spectral emissivity of materials at elevated temperatures. Analysis of pyrolytic gas products. Programmed heating and cooling cycles.
McDonnell Aircraft Corp., St. Louis 66, Missouri	K. Denney	Two 60-in parabolic reflectors	Carbon arc	1120 Btu/ft^2/sec	Evaluation of the oxidation resistance of tungsten alloys.

IMAGE FURNACE FACILITIES (Cont'd)

Name and Address	Investigators	Optical System	Source	Maximum Image Flux	Reactions and Experiments
U. S. A. (Cont'd)					
Narmco Research and Development, San Diego, Calif.	J. Chin B. Libbert		Carbon arc	240 cal/cm^2/sec	Incipient melting points of carbides. Vaporization rates and melting point determinations on silicon carbide. Effective heats of ablation and thermal diffusivity of graphite phenolics. Effective heats of ablation of teflon.
NASA, Ames Research Center, Moffett Field, Calif.	J. H. Lundell R. M. Wakefield E. J. DeFrance	Two 21-in elliptical reflectors	Carbon arc	325 cal/cm^2/sec	Determination of behavior of ablative heat-shield materials under radiative heating.
NASA, Langley Research Center, Langley Field, Virginia.	R. W. Peters R. G. Wilson M. A. Wallis	Double paraboloidal with 60-in mirrors	Carbon arc	1000 Btu/ft^2/sec 1/4-in dia. circular area.	Emissivity studies. Effects of pressure and heating rate on ablation materials.
NASA, Lewis Research Center, Cleveland, Ohio	C. E. May	21-inch ellipsoidal mirror	High pressure Xenon arc lamp		
National Bureau of Standards, Washington, D. C.	J. J. Diamond A. L. Dragoo R. F. Walker	Two 21-in ellipsoidal mirrors	Carbon arc	325 cal/cm^2/sec	Reaction of molten refractory oxides with various gases; vapor pressure of refractory oxides; rate of vaporization of refractory oxides as a function of ambient atmosphere; nature of species vaporizing from refractory oxides; nature of condensates from vaporizing refractories.
National Carbon Company Parma 30, Ohio	W. W. Lozier M. R. Null	Double ellipsoidal reflector	Carbon arc	15 w/mm^2 10 w/mm^2	High temperature material properties, emissivity, thermal conductivity, oxidation, and phase studies of graphite.
Naval Air Development Center, Johnsville, Pennsylvania	A. M. Stoll	36-in parabolic mirrors	Graphite heating element	33 cal/cm^2/sec	Study of the effects of thermal radiation on living tissue, design of protective devices against injury from heat sources.
Naval Material Laboratory, Brooklyn 1, New York	T. L. Monahan W. L. Derksen G. P. de Lhery	24-in dia. ellipsoidal first surface reflector	Carbon arc	340 cal/cm^2/sec	Study of thermal radiation burns.
Naval Radiological Defense Laboratory, San Francisco, Calif.	C. P. Butler	36-in double parbolic	Carbon arc	100 cal/cm^2/sec	Solar absorptance-emittance of coatings. Pyrolysis of cellulose; thermal properties of metals.
North American Aviation, Los Angeles, Calif.	R. H. Otto		Carbon arc	60 cal/cm^2/sec	
Pennsylvania State Univ., University Park, Pa.	F. Dachille	60-in parabolic clamshell arrangement	Carbon arc		Synthesis of compounds or solid solutions in refractory systems (theria and some rare oxides).
Quartermaster Research and Engineering Command, Natick, Mass.	E. S. Cotton	24-in ellipsoidal mirror 35-ft solar furnace	Tungsten lamp, carbon arc, Sun	6 cal/cm^2/sec tungsten lamp, 150 cal/cm^2/sec carbon arc, 100 cal/cm^2/sec solar furnace	Study of damage inflicted on various materials by exposure to thermal radiation.
Radio Corporation of America, Princeton, N. J.	M. W. Hopkins	Two 21-in ellipsoidal	Carbon arc	250 cal/cm^2/sec	Growth of single crystals of refractory oxides; solid state reactions at high temperature.
Solid State Materials Corporation, East Natick Mass.	J. B. Schroeder J. A. Adamski R. C. Linares J. F. Wenkus	Two 21-in elliptical mirrors	Carbon arc	325 cal/cm^2/sec	Growth of single crystals.
Southwest Research Institute, San Antonio, Texas	J. C. Cook G. Buss J. Baker	Twin paraboloid 37-in dia.	Carbon arc	700 cal/cm^2/sec average over 5/8-in dia. area	Thermophysical properties of materials.
Stanford Research Institute, Menlo Park, Calif.	R. E. De LaRue R. Sedlacek N. K. Hiester F. A. Halden R. S. Marcus	Two 16-in double elliptical and one 13-in double elliptical mirrors, and one 16-in and one 24-in paraboloidal concentrator	Three carbon arc and two solar furnaces	160 cal/cm^2/sec carbon arc; estimated 200 w^2/cm^2 solar furnace	Growth of single crystals; ignition studies of solid propellants; fire research, pyrolysis studies; oxidation studies; photochemistry.
Thiokol Chemical Corp., Elkton, Md.	F. W. Mueller G. Dolan	21-in ellipsoidal reflector	Carbon arc		Propellant ignition studies.
Thompson - Ramo Wooldridge Inc., Cleveland, Ohio	M. W. Mueller W. J. Leovic	21-in ellipsoidal reflectors	Carbon arc	325 cal/cm^2/sec	Cavity absorber and emissivity studies. High temperature coating materials; thermionic converter tests.
University of Arizona, Tucson, Arizona	U. N. Bentz	60-in paraboloid	Sun		
University of California, Berkeley, Calif.	T. N. Hazlett I. Pratt	60-in paraboidal mirrors	Tungsten Argon arc		
University of Utah, Salt Lake City, Utah	E. B. Christiansen	60-in paraboloidal reflector	Sun		Solid phase studies
University of Wisconsin, Madison, Wisconsin	J. L. Margrave		Sun		Investigation of evaporation and sublimation processes.
Wayne State University, Detroit, Michigan	R. F. Poplawsky J. E. Thomas, Jr.	Two 60-in parboloidal reflectors	Carbon arc		Growth of single crystals using floating zone technique.

IMAGE FURNACE FACILITIES (Cont'd)

Name and Address	Investigators	Optical System	Source	Maximum Image Flux	Reactions and Experiments
U. S. A. (Cont'd)					
Westinghouse Electric Corp., Lima, Ohio	A. J. Krauss	60-in paraboloidal reflector	Sun		Feasibility study of a solar heated thermo electric generator system using lithium hydride thermal storage.
John Yellott Engineering Associates, Phoenix, Arizona.	J. Yellott	60-in parabolic concentrator	Sun		Effects of thermal radiation on silicon cells.
U. S. S. R.					
Chemical Research Institute of the Armenian S. S. R.	M. G. Manvelyan A. Abbasarov S. Rustambekyan A. A. Badalyan	2, 615-m dia. paraboloidal mirror with heliostat	Sun		Study of halides
YUGOSLAVIA					
Metallurgical Institute, Ljubljana	J. Mastar	1.5-m parabolic concentrator	Sun		Synthesis of minerals.

DISTRIBUTION

Code	Addressee	No. of Copies
M6	AFCRL, OAR(CRXRA-Stop 39) L. G. Hanscom Field Bedford, Mass.	10
AF5	AFMTC (AFMTC Tech Library-MU-135) Patrick AFB, Fla.	1
AF 32	OAR (RROS, Col. John R. Fowler) Tempo D 4th and Independence Ave, Wash 25, D. C.	1
AF 33	AFOSR, OAR (SRYP) Tempo D 4th and Independence Ave, Washington 25, D. C.	1
AF 43	ASD (ASAPRD - Dist) Wright-Patterson AFB, Ohio	1
AF 124	RADC (RAALD) Griffiss AFB, New York Attn: Documents Library	1
AF 139	AF Missile Development Center (MDGRT) Holloman AFB, New Mexico	1
AF 314	Hq. OAR (RROSP, Maj. Richard W. Nelson) Washington 25, D. C.	1
AF 318	ARL (ARA-2) Library AFL 2292, Building 450 Wright-Patterson AFB, Ohio	1
Ar 5	Commanding General USASRDL Ft. Monmouth, N. J. Attn: Tech Doc. Ctr. SIGRA/SL-ADT	1
Ar 9	Department of the Army Office of the Chief Signal Officer Washington 25, D. C. Attn: SIGRD-4a-2	1

DISTRIBUTION (Cont'd)

Code	Addressee	No. of Copies
Ar 50	Commanding Officer Attn: ORDTL-012 Diamond Ordnance Fuze Laboratories Washington 25, D. C.	1
Ar 67	Redstone Scientific Information Center U. S. Army Missile Command Redstone Arsenal, Alabama	1
Ar 107	U. S. Army Aviation Human Research Unit U. S. Continental Army Command P. O. Box 428, Fort Rucker, Alabama Attn: Maj. Arne H. Eliasson	1
G 2	ASTIA (TIPAA) Arlington Hall Station Arlington 12, Virginia	10
G 31	Office of Scientific Intelligence Central Intelligence Agency 2430 E Street, N. W. Washington 25, D. C.	1
G 8	Library Boulder Laboratories National Bureau of Standards Boulder, Colorado	2
G 68	Scientific and Technical Information Facility Attn: NASA Representative (S-AK/DL) P. O. Box 5700 Bethesda, Maryland	1
G109	Director Langley Research Center National Aeronautics and Space Administration Langley Field, Virginia	1
N 9	Chief, Bureau of Naval Weapons Department of the Navy Washington 25, D. C. Attn: DLI-31	2

DISTRIBUTION (Cont'd)

Code	Addressee	No. of Copies
N 29	Director (Code 2027) U. S. Naval Research Laboratory Washington 25, D. C.	2
I 292	Director, USAF Project RAND The Rand Corporation 1700 Main Street Santa Monica, California THRU: AF Liaison Office	1
M 63	Institute of the Aerospace Sciences, Inc. 2 East 64th Street New York 21, New York Attn: Librarian	1
U 32	Massachusetts Institute of Technology Research Laboratory Building 26, Room 327 Cambridge 39, Massachusetts Attn: John H. Hewitt	1
	A. Shores (Avco Holloman AFB) New Mexico	1
	Dr. Paul D. Jose Directorate of Research Analysis SRLS Air Force Office of Scientific Research United States Air Force Holloman Air Force Base, New Mexico	1
	Lt. Col. Ralph W. Conners Chief Solid State Sciences AFOSR Att. SRPS Washington 25, D. C.	1
	Mr. Murray Klamkin Division of Interdisciplinary Studies and Research University of Buffalo Buffalo 26, N. Y.	1
	Max Swerdlow AFOSR Attn: SRPS Washington 25, D. C.	1

Code	Addressee
	Dr. Nevin K. Hiester, Manager Stanford Research Institute Menlo Park, California
	Mr. Clay P. Butler Radiation Characteristics and Effects Br. U. S. Naval Radiological Laboratory, San Francisco 24, California
	Brig. Gen. Harold Walmsley Assoc. for Applied Solar Energy Arizona State University Tempe, Arizona
	Central Files
	Document Control
	Research Library